THE ASTRONOMICAL JOURNAL, 119:2645–2663, 2000 June

STRUCTURAL AND PHOTOMETRIC CLASSIFICATION OF GALAXIES. I. CALIBRATION BASED ON A NEARBY GALAXY SAMPLE

MATTHEW A. BERSHADY
Department of Astronomy, University of Wisconsin, 475 North Charter Street, Madison, WI 53706; mab@astro.wisc.edu
ANNA JANGREN
Department of Astronomy and Astrophysics, Pennsylvania State University, 525 Davey Laboratory, University Park, PA 16802; jangren@astro.psu.edu
AND
CHRISTOPHER J. CONSELICE
Department of Astronomy, University of Wisconsin, 475 North Charter Street, Madison, WI 53706; chris@astro.wisc.edu
Received 1999 August 30; accepted 2000 February 11

ABSTRACT

In this paper we define an observationally robust, multiparameter space for the classification of nearby and distant galaxies. The parameters include luminosity, color, and the image-structure parameters: size, image concentration, asymmetry, and surface brightness. Based on an initial calibration of this parameter space using the "normal" Hubble types surveyed in 1996 by Frei et al., we find that only a subset of the parameters provide useful classification boundaries for this sample. Interestingly, this subset does not include distance-dependent scale parameters such as size or luminosity. The essential ingredient is the combination of a spectral index (e.g., color) with parameters of image structure and scale: concentration, asymmetry, and surface brightness. We refer to the image structure parameters (concentration and asymmetry) as indices of "form." We define a preliminary classification based on spectral index, form, and surface brightness (a scale) that successfully separates normal galaxies into three classes. We intentionally identify these classes with the familiar labels of early, intermediate, and late. This classification, or others based on the above four parameters, can be used reliably to define comparable samples over a broad range in redshift. The size and luminosity distribution of such samples will not be biased by this selection process except through astrophysical correlations between spectral index, form, and surface brightness.

Key words: galaxies: compact — galaxies: fundamental parameters — galaxies: starburst

1. INTRODUCTION

It is now well established that a large fraction of galaxies discovered at intermediate and high redshift have unusual morphologies and thus cannot be classified in terms of the nominal Hubble-Sandage system (Driver, Windhorst, & Griffiths 1995; Driver et al. 1998; Abraham et al. 1996a, 1996b). The Hubble classification scheme is also difficult to apply to many local galaxies, dubbed "peculiar," or any galaxies imaged at low signal-to-noise (S/N) or apparently small size (relative to the point-spread function). The Hubble-Sandage classification system was predicated on the study of nearby "normal" galaxies—luminous and relatively quiescent objects (Sandage 1961, Sandage & Tamman 1987, Sandage & Bedke 1993). While the classification system developed by de Vaucouleurs et al. (1976) makes an attempt to push the framework to "later" types, it still suffers from the above shortcomings. Fundamentally, these traditional classification schemes are based on the concept of pigeon-holing galaxies based on a reference set, or archetypes. These archetypes are selected from samples in the local universe and are preferentially axisymmetric systems. Since our local census is undoubtedly incomplete and since galaxies evolve, such reference sets by their very definition are incomplete. Thus it is not surprising that these systems are of marginal utility in the study of dwarf galaxies, interacting galaxies, or galaxies at high redshift.

An alternative classification scheme could be based on quantitative indices, the interrelation of which is not predetermined by a finite reference set. This would permit galaxies to be classified, for example, in different stages of their evolution; albeit the classification would be different but the basis set of indices would be the same. The goal of this paper is to define such a set of indices that can be used as quantitative, objective classifiers of galaxies (1) over a wide range in redshift and (2) for wide range of galaxy types. In particular, we desire classifiers that are well suited to typing both "normal" galaxies and the compact galaxies that are the focus of a companion study (Jangren et al. 2000, hereafter Paper II). We anticipate that such a classification scheme is both necessary and enabling for the exploration of the physical mechanisms driving galaxy evolution (Bershady 1999).

What are the desired characteristics of classification parameters? They should be physically interesting (closely related to underlying physical properties of galaxies), model independent, and measurable for all galaxy types. It also should be possible to accurately determine the parameters chosen for a wide range of image resolution and signal-to-noise ratios.

From Hubble's classification a posteriori we have learned that a strong correlation exists between galaxy spectral type and apparent morphological features—at least for the galaxy types that fit well within his scheme. This correlation—noted by Hubble as early as 1936 (Hubble 1936)—can loosely be termed a color-morphology relation, although the correlation is not necessarily limited to broadband color. This is a triumph of Hubble's classification explicitly because it is not part *of* the classification. Furthermore, the correlation yields clues about the physical connection of the present matter distribution and the star formation histories in galaxies. But while morphology (or form) and spectral type are correlated, there is also significant dispersion in this correlation. Some of the more notable deviations from the nominal color-morphology relation are found in the plethora of forms for spectrally "late"-type galaxies, the presence of E+A galaxies (Dressler & Gunn 1993), and the compact luminous blue emission-line galaxies studied in Paper II (as we shall show). This points to the importance of form and spectral type as key, yet independent, axes of a revised classification system.

However, the only example of such a revised classification system is that of Morgan (1958, 1959), where central light concentration is used as the primary classification parameter. Morgan was motivated by the facts that (1) a salient criterion used in classifying galaxies in the Hubble-Sandage system is the degree of central concentration of light, (2) there was a significant dispersion in spectral type and Hubble type (Humason, Mayall, & Sandage 1956), and (3) spectral type appeared to correlate more strongly with light concentration. In this way, Morgan hoped to wed the classification of stellar populations to the classification of galaxies. Nonetheless, he was compelled to introduce a secondary parameter, i.e., the "form family," because there was still a dispersion of morphological forms within each of his spectral types. Today, one should be able to improve upon Morgan's scheme by introducing quantitative measures of image concentration and other indices of form and by independently assessing the spectral type via colors or spectra.

A number of subsequent attempts have been made to construct quantitative classification system that could replace or modify the current Hubble scheme. Yet these schemes are generally based purely either on photometric form (e.g., Elmegreen & Elmegreen 1982; Okamura et al. 1984; Watanabe, Kodaira, & Okamura. 1985; Doi, Fukugita, & Okamura 1993; Abraham et al. 1994; Odewahn 1995; Han 1995) or spectral type (e.g., Bershady 1995; Connolly et al. 1995; Zaritsky, Zabludoff, & Willick 1995; Folkes, Lahav, & Maddox 1996; Bromley et al. 1998; Ronen, Aragón-Salamanca, & Lahav 1999). In essence, they have relied implicitly on an assumed correlation between galaxy spectral type and apparent morphology. Related attempts have been made to use artificial neural networks to reproduce the Hubble scheme in an objective way (e.g., Burda & Feitzinger 1992; Storrie-Lombardi et al. 1992; Spiekermann 1992; Serra-Ricart et al. 1993; Naim et al. 1995; Odewahn 1995; Odewahn et al. 1996). Yet these go no further in differentiating between spectral type and form. Only in Whitmore's (1984) scheme are spectral and structural parameters combined; i.e., $B-H$ color, size, and bulge-to-total ratio are used to define two principal classification axes of *scale* and *form*. But again, the correlation(s) between galaxy spectral type, scale, and form are not explicit.

Here we attempt to expand on Morgan's program by fully quantifying the classification of form via image concentration and several other structural parameters, and explicitly using color as an indicator of spectral type. In this study we choose to use only a single color ($B-V$), but we anticipate that a more desirable future development would be to include broadwavelength coverage, multicolor data, and spectroscopic line indices. Spectroscopic line indices would be required, for example, to identify E+A galaxies. While such galaxies are not the focus of the present work, a comprehensive classification scheme should be able to isolate these systems and determine the range of their morphology (see Dressler & Gunn 1992, Couch et al. 1994, and Wirth, Koo, & Kron 1994). Nonetheless, broadband colors are a cost-effective way to characterize the spectral continuum (see Bershady 1995 and Connolly et al. 1995). Of more direct relevance to the study at hand, a future elaboration including $U-V$ and $V-K$ would enhance the ability to distinguish between spectral types, particularly for galaxies with extremely blue optical colors (e.g., Aaronson 1978; Bershady 1995).

We have also chosen to quantify form and scale via nonparametric measures, such as luminosity, half-light size and surface brightness, asymmetry, and image concentration. An alternative, model-dependent approach is to decompose a galaxy's light profile into a disk and bulge. The traditional one-dimensional decompositions are fraught with technical problems, such that decompositions can only be achieved reliably for about half of all disk galaxies (Kent 1985). The newer two-dimensional decomposition techniques are superior (e.g., de Jong 1996b) and have been shown to successfully reproduce observed light profiles for faint galaxies (e.g., Simard et al. 1999). Indeed, one can argue that two-dimensional model fitting to imaging data is optimum in terms of using the available information and for minimizing random error. At high S/N and high angular resolution, however, even the most "normal" galaxies exhibit peculiarities (as discussed in more detail in § 3.3.2), such that simple bulge-plus-disk models cannot reproduce these frequently observed peculiarities in light distributions with high fidelity. The situation worsens for "peculiar" galaxies. For this reason we have some concerns about the uniqueness of the observationally derived model parameters and hence about their interpretation. We anticipate future developments that use the models and nonparametric measurements in a hybrid scheme optimal for characterizing galaxy light distributions both in terms of random and systematic errors.

It is worth noting again that bright galaxy samples are notorious for missing or underrepresenting certain galaxy types—particularly dwarfs and low surface brightness galaxies. The samples used here are no exception. While this was one of our complaints about the classical Hubble scheme, there are two key differences with our approach: (1) the classification parameters we develop are objective, and (2) these parameters do not assume the presence of basic axisymmetry, disk-plus-bulge structure, or spiral patterns, which underly the Hubble scheme. As we will show, the galaxies examined here are sufficiently diverse to establish the *parameter space* for a comprehensive classification scheme, although not the comprehensive classification itself. By developing an initial classification of these galaxies, however, we intend to use it as a foil against which we can begin to compare the classification of more distant samples: How are the classifications different? Do the nearby and distant samples occupy the same regions of parameter space? If not, do the differences represent continuous extensions of these parameters, or are they physically disjoint? These are the types of questions one can address given the limitations of current local samples. Note that we must stop short of identifying differences as "new" epoch-specific classes of galaxies. Without a complete census of both the nearby and distant universe, it is not possible to establish whether there are different classes of galaxies at different redshifts; apparent differences could simply be artifacts of the presently limited samples. With such a complete census, in the future we may hope to address the deeper issue of how the comoving space densities of different classes evolve.

Toward the goal of establishing a comprehensive classification scheme of utility to distant galaxy studies, in this paper we assemble a robust set of nonparametric, photometric and structural properties for a range of nearby luminous galaxies. We define a multivariate photometric parameter space that forms an initial classification scheme for these galaxies. This classification can be used reliably to identify comparable samples in other surveys and at higher redshift. In the accompanying paper (Paper II) we measure these properties for compact, luminous emission-line galaxies at intermediate redshift, compare them with the "normal" nearby galaxies studied here, and demonstrate that our classification parameter space distinguishes between these two samples. We discuss the implications for the evolution of this intermediate-redshift sample therein. In future papers in this series we intend to extend our analysis (1) to more representative samples of the local volume that include dwarf and emission-line galaxies (e.g., the University of Michigan Objective Prism Survey; Salzer et al. 1989), (2) to more comprehensive samples of distant galaxies (e.g., magnitude-limited samples from the Hubble Deep Field), and (3) to studies of the morphological evolution of these distant samples. The classification scheme that we propose here is intended as a framework for these future studies.

The data sets are presented in § 2; the analysis is described in § 3. The results are presented in § 4 and summarized in § 5. Throughout this paper we adopt $H_0 = 50$ km s^{-1} Mpc^{-1}, $q_0 = 0.1, \Lambda = 0$.

2. NEARBY GALAXY SAMPLES

As a primary reference sample, 101 of the 113 local Hubble-type galaxies from the catalog of Frei et al. (1996) were analyzed. This sample will define what we mean by "normal" galaxies in this paper. This catalog is the only digital multiband sample publicly available that is reasonably comprehensive; it consists of ground-based CCD images of bright galaxies, all apparently large (most have diameters of 4′–6′) and well resolved. As a result the sample contains mostly luminous and physically large galaxies: out of the 101 objects we used in our analysis, only seven have $L < 0.1\ L^*$. We excluded 12 objects whose apparent sizes were larger than the CCD field of view (thus their image structure parameters could not be well estimated). Two of the excluded objects are early-type galaxies (E–S0), seven are intermediate (Sa–Sb), and three are late-type (Sc–Irr).[1] The majority of the remaining sample are spirals and S0 galaxies. Frei et al. have removed foreground stars from the images of the nearby galaxies, in a few cases leaving visible scars; except in the case of NGC 5792, these residuals did not cause noticeable problems when determining the structural parameters (§ 3.3).

In several instances in the present analysis we reference the sample of Kent (1984, 1985), which is composed of 53 nearby, luminous, and physically large galaxies similar to the Frei et al. sample. We find Kent's sample useful for comparison of both photometric and structural parameters. We also reference the sample of 196 normal (nonactive) Markarian galaxies studied by Huchra (1977a). Relevant characteristics of the above three samples are summarized in Table 1, including an enumeration of the effective filter systems used in each study. Further details on these photometric systems are found in the studies listed in the table and references therein.

2.1. *Comparison of Reference Samples with Emission-Line Galaxy Samples*

Both the Frei et al. and Kent samples are underrepresentative of dwarf galaxies and contain neither H II galaxies nor low surface brightness galaxies. The latter objects have been shown to make up a significant fraction of the local galaxy population (de Jong 1995, 1996a). Clearly our reference samples do not constitute a representative template of the local population. Here we estimate where these samples may be particularly unrepresentative with an eye toward the study of faint galaxy samples in future papers. In Figures 1 and 2 we compare the Frei et al. samples photometric properties of color and luminosity with (1) the normal Markarian galaxies (Huchra 1977a), (2) dwarf spheroidals (as described in the following section), and (3) the intermediate-redshift samples presented in Paper II.

Since the Markarian galaxies were selected from objective prism plates based on their strong UV continua, the sample is biased toward bluer colors than the Frei et al. galaxies and is thus likely more representative of star-forming galaxies. Huchra's sample contains fainter galaxies that extend the magnitude range down to $M_B \sim -14$ and the color-color locus blueward of $B-V = 0.4$.

The intermediate-redshift galaxies, also selected in part because of their blue color (see Paper II), have blue luminosities comparable to the brighter half of the Frei et al. sample, but with bluer colors. This places most of them in a distinct region of the color-luminosity plot from the Frei et al. sample. In contrast, the distribution of the Markarian galaxies extends into the region occupied by the intermediate-redshift objects. In the color-color diagram, again the intermediate-redshift galaxies largely overlap with

TABLE 1

NEARBY GALAXY DATA SETS

Survey	N	Distance	Telescope	Filters
Frei et al. (1996)......	72	≤41 Mpc	Lowell 1.1 m	B_J, R
	29	≤19 Mpc	Palomar 1.3 m	gri
Kent (1984)	53	≤65 Mpc	Whipple 0.6 m	r
Huchra (1977a).......	196	≤286 Mpc	Mount Wilson 2.5 m, Palomar 1.5 m	UBV

---

[1] The excluded objects are: NGC 2403, 2683, 3031, 3079, 3351, 3623, 4406, 4472, 4594, 4826, 5746, and 6503.

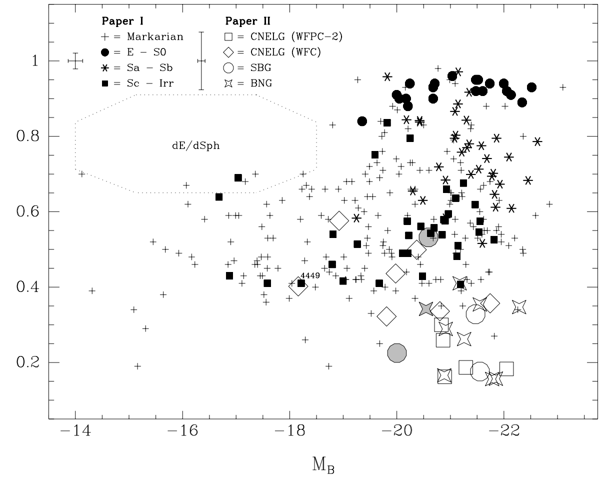

FIG. 1.—Rest-frame $B-V$ vs. M_B for the nearby galaxy samples of Frei et al. and Kent (E–S0, Sa–Sb, and Sc–Irr) and Huchra's (1977a) samples of normal Markarian galaxies (plus signs). The dotted outline indicates the approximate locus of dE/dSph galaxies. The intermediate-redshift samples from Paper II are also plotted for comparison: blue nucleated galaxies (BNGs), compact, narrow emission-line galaxies (CNELGs), and small, blue galaxies (SBGs). (The two SBGs and the BNG that we ultimately determine not to be "luminous blue compact galaxies" in Paper II are shown as hatched symbols.) Only a few Markarian galaxies and late-type galaxies from the Frei et al. and Kent catalog share the extreme color–magnitude properties of the intermediate-redshift objects. In this plot, and in Figs. 2–6, the vigorously star-forming galaxy NGC 4449 is labeled. Characteristic random errors are indicated separately for the Frei et al. sample and the intermediate-z objects.

the Markarian sample in the region corresponding to extreme blue colors *not* occupied by the Frei et al. or Kent samples.

In short, the Frei et al. sample is spectro-photometrically disjoint from extreme samples of blue star-forming galaxies at intermediate redshift (e.g., Paper II), even though both contain intrinsically luminous and moderate to high surface brightness systems. Yet clearly there are local examples (e.g., from Markarian) which are as blue and luminous as these intermediate-redshift, star-forming galaxies. These sources are simply missing from the Frei et al. sample. The comparison of the global properties of the intermediate-redshift, compact, star-forming galaxies in Paper II to those of local galaxies from Frei et al. (here) is then an initial step in mapping the range of galaxy types at any redshift. Further investigation of the nature and evolution of these types of extreme, star-forming systems will be greatly facilitated by future work quantifying the image structure of local counterparts $B-V < 0.4$ and $M_B < -19$.

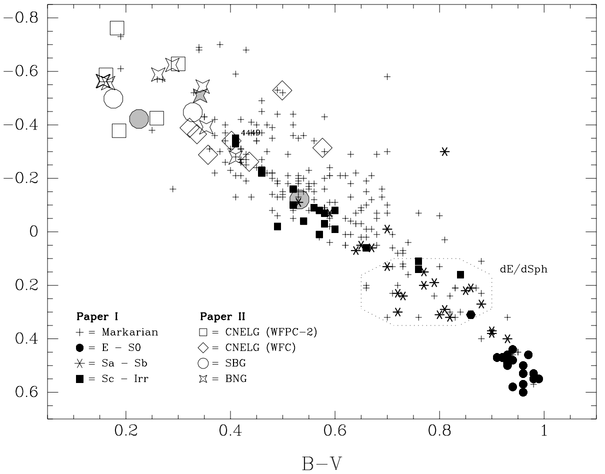

FIG. 2.—Rest-frame $U-B$ vs. $B-V$ for the samples as in Fig. 1. The intermediate-redshift samples of Paper II largely overlap with the bluest Markarian galaxies, which extend blueward the color-color relation seen for the "normal" galaxies from Frei et al. and Kent.

2.2. *Comparison of Reference Samples with Dwarf Spheroidals*

We have made some attempt where possible to access the photometric and structural properties of other key dwarf populations. We schematically indicate the locus of dwarf ellipticals/spheroidals in Figures 1 and 2, using data from Caldwell (1983), Bingelli & Cameron (1991), and Bingelli & Jerjen (1998). The dwarf spheroidals occupy a virtually unpopulated region of the color-luminosity diagram at relatively red colors and low luminosity. The absence of such objects from most surveys is attributed typically to a selection bias since these sources are at low surface brightness. It is interesting to note that in the color-color diagram the dwarf spheroidals occupy a region overlapping with the early- to intermediate-type spirals. Hence the integrated broadband light of these systems is unusual compared with our reference samples only with respect to their luminosity. We refer to the dwarf spheroidal properties extensively in future papers, where we also explore their image structural properties.

3. ANALYSIS

As noted in the introduction, many galaxies are sufficiently unusual that they cannot be classified in terms of the normal Hubble scheme. This becomes increasingly true at intermediate redshifts. The compact luminous emission-line galaxies in Paper II are such an example. This is not due to poor spatial resolution, but to truly unusual morphological properties, e.g., off-centered nuclei, tails, asymmetric envelopes, etc. To compare such objects morphologically to "normal" galaxies, we define here six fundamental parameters of galaxy type that are quantitative, can be reliably determined over a range in redshift, and are physically meaningful.

Two of these parameters are photometric, derived from existing ground-based imaging and estimated k-corrections: rest-frame color ($B-V$) and absolute blue luminosity (M_B). Two are image structure parameters, derived from multiaperture photometric analysis presented below: physical half-light radius (R_e) and image concentration (C). One is a combined photometric-structural parameter: average rest-frame surface brightness (SB_e) within R_e. Of the three parameters luminosity, half-light radius, and surface brightness, any one can obviously be derived from the other two. (We consider all three since in any given range of, e.g., luminosity, there is significant dispersion in both SB_e and R_e.) The sixth parameter, a 180° rotational asymmetry index (A), utilizes the multiaperture photometry indirectly through definition of the extraction radius for rotation; we refer to A as a structural parameter. Table 2 contains all individual measurements for the Frei et al. sources. Luminosities and all image-structure parameters are measured in the rest-frame B band.

TABLE 2

LOCAL GALAXY PROPERTIES

NGC (1)	Type (2)	M_B (3)	$B-V$ (4)	SB_e (5)	R_e (6)	$r_{\eta = 0.2}$ (7)	C (8)	A (9)
2541......	6	−19.00 ± 0.14	0.42 ± 0.20	22.86 ± 0.15	4.55 ± 0.07	126.5 ± 1.1	3.06 ± 0.04	0.16 ± 0.10
2715......	5	−20.63 ± 0.20	0.54 ± 0.20	21.56 ± 0.25	5.31 ± 0.35	90.1 ± 0.5	2.64 ± 0.01	0.23 ± 0.02
2768......	−5	−22.05 ± 0.23	0.92 ± 0.14	20.92 ± 0.31	7.62 ± 0.73	118.4 ± 0.8	4.19 ± 0.01	0.02 ± 0.01
2775......	2	−21.09 ± 0.17	0.87 ± 0.14	20.82 ± 0.23	4.65 ± 0.31	88.1 ± 0.7	3.96 ± 0.01	0.07 ± 0.01
2903......	4	−20.30 ± 0.12	0.66 ± 0.14	20.95 ± 0.13	3.44 ± 0.09	154.4 ± 0.2	3.08 ± 0.01	0.22 ± 0.01
2976......	5	−16.68 ± 0.37	0.64 ± 0.18	21.56 ± 0.50	0.86 ± 0.22	113.2 ± 0.2	2.53 ± 0.01	0.20 ± 0.01
2985......	2	−21.53 ± 0.12	0.71 ± 0.12	19.82 ± 0.14	3.61 ± 0.14	68.2 ± 0.3	3.85 ± 0.04	0.05 ± 0.03
3077......	12	−17.04 ± 0.37	0.69 ± 0.18	21.15 ± 0.50	0.84 ± 0.21	134.7 ± 0.4	3.95 ± 0.01	0.25 ± 0.01
3147......	4	−22.63 ± 0.17	0.79 ± 0.23	21.44 ± 0.18	12.57 ± 0.38	94.8 ± 0.9	3.77 ± 0.04	0.09 ± 0.04
3166......	0	−21.35 ± 0.13	0.92 ± 0.14	19.82 ± 0.15	3.32 ± 0.12	48.5 ± 1.1	4.47 ± 0.02	0.07 ± 0.02
3184......	6	−20.19 ± 0.10	0.58 ± 0.14	22.51 ± 0.11	6.73 ± 0.09	56.3 ± 1.9	2.38 ± 0.01	0.24 ± 0.04
3198......	5	−20.22 ± 0.10	0.54 ± 0.14	22.26 ± 0.11	6.06 ± 0.07	175.0 ± 1.1	3.36 ± 0.02	0.14 ± 0.05
3319......	6	−19.67 ± 0.17	0.41 ± 0.25	22.71 ± 0.17	5.80 ± 0.09	159.5 ± 0.5	2.88 ± 0.04	0.13 ± 0.09
3344......	4	−19.25 ± 0.13	0.58 ± 0.18	21.83 ± 0.14	3.17 ± 0.04	144.8 ± 0.3	2.67 ± 0.01	0.15 ± 0.03
3368......	2	−20.43 ± 0.13	0.84 ± 0.18	20.14 ± 0.13	2.51 ± 0.03	94.3 ± 0.3	3.67 ± 0.01	0.09 ± 0.01
3377......	−5	−19.35 ± 0.16	0.84 ± 0.14	19.97 ± 0.20	1.42 ± 0.08	60.7 ± 0.6	4.47 ± 0.03	0.03 ± 0.02
3379......	−5	−20.24 ± 0.07	0.94 ± 0.04	19.69 ± 0.10	1.88 ± 0.06	77.2 ± 0.3	4.52 ± 0.01	0.02 ± 0.01
3486......	5	−19.26 ± 0.10	0.51 ± 0.14	21.41 ± 0.11	2.63 ± 0.04	140.4 ± 0.7	3.52 ± 0.01	0.16 ± 0.01
3556......	6	−20.93 ± 0.10	0.66 ± 0.14	22.10 ± 0.10	8.21 ± 0.14	55.9 ± 0.6	2.62 ± 0.01	0.26 ± 0.02
3596......	5	−20.96 ± 0.15	...	21.31 ± 0.15	5.50 ± 0.05	62.2 ± 0.2	2.69 ± 0.01	0.18 ± 0.02
3631......	5	−21.55 ± 0.08	0.58 ± 0.12	21.88 ± 0.08	9.38 ± 0.07	113.6 ± 0.2	3.23 ± 0.02	0.23 ± 0.01
3672......	5	−21.24 ± 0.15	0.68 ± 0.21	21.90 ± 0.15	8.22 ± 0.05	87.3 ± 0.3	2.82 ± 0.01	0.27 ± 0.02
3675......	3	−20.51 ± 0.15	...	22.69 ± 0.16	8.45 ± 0.12	144.8 ± 0.9	4.02 ± 0.02	0.25 ± 0.03
3726......	5	−21.12 ± 0.07	0.48 ± 0.11	21.95 ± 0.08	7.96 ± 0.09	133.5 ± 0.3	2.36 ± 0.01	0.23 ± 0.04
3810......	5	−20.84 ± 0.11	0.54 ± 0.14	21.08 ± 0.11	4.70 ± 0.07	90.9 ± 0.2	3.10 ± 0.01	0.22 ± 0.01
3877......	5	−20.25 ± 0.10	0.80 ± 0.14	22.01 ± 0.11	5.46 ± 0.06	104.6 ± 0.6	3.59 ± 0.01	0.24 ± 0.01
3893......	5	−21.04 ± 0.15	...	20.72 ± 0.15	4.35 ± 0.04	75.1 ± 0.1	3.10 ± 0.01	0.25 ± 0.01
3938......	5	−21.14 ± 0.10	0.51 ± 0.14	21.55 ± 0.10	6.67 ± 0.05	124.3 ± 0.3	2.65 ± 0.01	0.20 ± 0.01
3953......	4	−21.21 ± 0.10	0.76 ± 0.14	21.49 ± 0.10	6.71 ± 0.06	126.0 ± 0.2	3.25 ± 0.01	0.16 ± 0.01
4013......	3	−19.82 ± 0.11	0.96 ± 0.16	23.71 ± 0.12	9.81 ± 0.14	63.0 ± 0.3	2.13 ± 0.03	0.03 ± 0.10
4030......	4	−21.58 ± 0.17	...	21.10 ± 0.17	6.63 ± 0.07	83.0 ± 0.2	3.44 ± 0.01	0.15 ± 0.01
4088......	4	−20.91 ± 0.09	0.58 ± 0.13	21.64 ± 0.10	6.25 ± 0.07	111.7 ± 0.5	2.71 ± 0.01	0.43 ± 0.01
4123......	5	−20.96 ± 0.11	0.59 ± 0.16	22.52 ± 0.11	9.60 ± 0.08	105.5 ± 0.8	2.70 ± 0.02	0.18 ± 0.02
4125......	−5	−22.13 ± 0.13	0.91 ± 0.18	20.65 ± 0.14	6.95 ± 0.12	117.2 ± 1.5	4.31 ± 0.03	0.04 ± 0.01
4136......	5	−19.15 ± 0.17	...	22.07 ± 0.17	3.39 ± 0.05	101.3 ± 0.4	2.81 ± 0.02	0.18 ± 0.02
4144......	6	−16.87 ± 0.15	0.43 ± 0.18	22.28 ± 0.17	1.31 ± 0.05	119.1 ± 1.2	3.40 ± 0.02	0.17 ± 0.02
4157......	5	−20.88 ± 0.10	0.58 ± 0.14	21.28 ± 0.11	5.23 ± 0.08	104.6 ± 1.9	3.58 ± 0.04	0.27 ± 0.04
4178......	8	−20.10 ± 0.11	0.49 ± 0.11	22.25 ± 0.14	5.72 ± 0.23	116.5 ± 0.4	2.65 ± 0.02	0.24 ± 0.05
4189......	6	−19.59 ± 0.07	0.75 ± 0.10	21.92 ± 0.07	3.89 ± 0.06	63.1 ± 0.2	2.33 ± 0.02	0.33 ± 0.03
4192......	2	−21.31 ± 0.17	0.77 ± 0.11	22.11 ± 0.23	9.32 ± 0.81	183.2 ± 0.6	3.54 ± 0.28	0.25 ± 0.03
4216......	3	−21.15 ± 0.19	0.97 ± 0.11	21.41 ± 0.26	6.28 ± 0.50	164.7 ± 0.6	5.03 ± 0.01	0.28 ± 0.01
4242......	8	−18.81 ± 0.17	0.54 ± 0.23	23.50 ± 0.17	5.60 ± 0.19	294.2 ± 2.5	3.13 ± 0.11	0.15 ± 0.07
4254......	5	−21.82 ± 0.08	0.53 ± 0.11	20.90 ± 0.08	6.75 ± 0.05	133.1 ± 0.1	3.07 ± 0.01	0.36 ± 0.01
4258......	4	−20.91 ± 0.08	0.68 ± 0.11	21.10 ± 0.08	4.87 ± 0.08	238.0 ± 0.5	3.42 ± 0.00	0.23 ± 0.01
4303......	4	−21.60 ± 0.09	0.52 ± 0.13	20.98 ± 0.09	6.33 ± 0.02	131.5 ± 0.3	2.73 ± 0.01	0.30 ± 0.01
4321......	4	−21.92 ± 0.08	0.67 ± 0.11	22.07 ± 0.08	12.16 ± 0.04	194.7 ± 0.3	2.93 ± 0.01	0.18 ± 0.03
4340......	−1	−20.00 ± 0.19	0.91 ± 0.07	21.26 ± 0.27	3.45 ± 0.30	65.8 ± 0.3	4.27 ± 0.02	0.01 ± 0.01
4365......	−5	−21.52 ± 0.08	0.95 ± 0.08	20.42 ± 0.09	4.72 ± 0.12	108.8 ± 1.0	4.24 ± 0.03	0.00 ± 0.02
4374......	−5	−22.00 ± 0.06	0.94 ± 0.07	21.21 ± 0.08	8.46 ± 0.16	179.6 ± 1.9	5.01 ± 0.02	0.01 ± 0.01
4394......	3	−20.42 ± 0.09	0.84 ± 0.13	21.42 ± 0.10	4.52 ± 0.05	93.7 ± 0.2	4.23 ± 0.02	0.06 ± 0.01
4414......	5	−19.82 ± 0.14	0.84 ± 0.18	20.65 ± 0.16	2.40 ± 0.07	78.7 ± 0.2	3.54 ± 0.01	0.21 ± 0.01
4429......	−1	−21.04 ± 0.14	0.96 ± 0.08	20.77 ± 0.19	4.44 ± 0.26	95.8 ± 0.6	3.62 ± 0.02	0.05 ± 0.02
4442......	−2	−20.68 ± 0.19	0.93 ± 0.11	19.52 ± 0.26	2.12 ± 0.17	39.6 ± 0.5	4.08 ± 0.02	0.05 ± 0.02
4449......	10	−18.21 ± 0.14	0.41 ± 0.18	20.42 ± 0.15	1.03 ± 0.03	108.6 ± 0.2	3.07 ± 0.01	0.29 ± 0.01
4450......	2	−21.10 ± 0.08	0.80 ± 0.11	21.62 ± 0.08	6.77 ± 0.05	127.2 ± 0.6	3.88 ± 0.02	0.06 ± 0.01
4477......	−3	−20.71 ± 0.14	0.94 ± 0.07	20.70 ± 0.19	3.69 ± 0.22	81.2 ± 0.3	4.24 ± 0.01	0.01 ± 0.01
4486......	−4	−22.52 ± 0.05	0.93 ± 0.06	20.20 ± 0.06	6.75 ± 0.09	137.6 ± 0.6	4.05 ± 0.01	0.02 ± 0.01
4487......	6	−20.82 ± 0.24	...	21.69 ± 0.24	6.14 ± 0.14	96.8 ± 0.4	2.62 ± 0.02	0.13 ± 0.05
4498......	7	−19.30 ± 0.15	...	22.15 ± 0.16	3.77 ± 0.05	67.6 ± 0.5	2.88 ± 0.03	0.16 ± 0.04
4501......	3	−21.77 ± 0.04	0.69 ± 0.06	21.49 ± 0.04	8.69 ± 0.06	149.3 ± 0.2	3.50 ± 0.01	0.21 ± 0.02
4526......	−2	−21.48 ± 0.14	0.95 ± 0.08	19.88 ± 0.19	3.61 ± 0.21	73.1 ± 0.7	3.99 ± 0.01	0.07 ± 0.01
4527......	4	−20.18 ± 0.08	0.84 ± 0.12	22.48 ± 0.08	6.59 ± 0.04	148.2 ± 0.5	3.93 ± 0.01	0.25 ± 0.03
4535......	5	−21.46 ± 0.08	0.62 ± 0.12	22.21 ± 0.08	10.49 ± 0.05	191.2 ± 0.3	2.46 ± 0.01	0.15 ± 0.04
4548......	3	−21.08 ± 0.08	0.80 ± 0.10	22.47 ± 0.10	9.91 ± 0.21	161.6 ± 0.4	3.73 ± 0.01	0.08 ± 0.03

TABLE 2—*Continued*

NGC (1)	Type (2)	M_B (3)	$B-V$ (4)	SB$_e$ (5)	R_e (6)	$r_{\eta=0.2}$ (7)	C (8)	A (9)
4559......	6	−20.48 ± 0.11	0.43 ± 0.16	21.12 ± 0.12	4.05 ± 0.05	135.4 ± 0.2	2.71 ± 0.01	0.22 ± 0.03
4564......	−5	−20.05 ± 0.09	0.90 ± 0.07	20.31 ± 0.11	2.28 ± 0.08	46.0 ± 0.7	4.38 ± 0.04	0.02 ± 0.03
4569......	2	−21.80 ± 0.18	0.70 ± 0.11	21.82 ± 0.24	10.23 ± 0.75	179.4 ± 0.8	3.39 ± 0.01	0.15 ± 0.03
4571......	7	−20.21 ± 0.17	0.49 ± 0.10	22.59 ± 0.23	7.02 ± 0.51	111.0 ± 0.4	2.73 ± 0.02	0.08 ± 0.07
4579......	3	−21.58 ± 0.10	0.78 ± 0.11	21.25 ± 0.11	7.13 ± 0.18	135.5 ± 0.4	3.97 ± 0.01	0.06 ± 0.02
4593......	3	−22.25 ± 0.25	...	21.38 ± 0.30	10.32 ± 0.73	96.7 ± 0.5	3.98 ± 0.02	0.09 ± 0.01
4621......	−5	−21.48 ± 0.22	0.92 ± 0.08	19.46 ± 0.30	2.98 ± 0.28	60.0 ± 0.3	4.17 ± 0.02	0.01 ± 0.01
4636......	−5	−21.60 ± 0.12	0.92 ± 0.14	20.84 ± 0.13	5.95 ± 0.16	133.5 ± 0.4	3.89 ± 0.01	0.01 ± 0.01
4651......	5	−20.7 ± 0.10	0.56 ± 0.12	21.78 ± 0.12	6.04 ± 0.19	103.6 ± 1.1	4.34 ± 0.02	0.11 ± 0.03
4654......	6	−20.90 ± 0.10	0.58 ± 0.14	21.76 ± 0.10	6.58 ± 0.07	106.8 ± 0.3	2.75 ± 0.02	0.20 ± 0.04
4689......	4	−20.48 ± 0.14	0.63 ± 0.11	22.87 ± 0.17	9.06 ± 0.46	149.3 ± 1.7	3.66 ± 0.03	0.07 ± 0.08
4710......	−1	−20.21 ± 0.14	0.88 ± 0.18	21.50 ± 0.15	4.25 ± 0.09	77.2 ± 0.3	3.33 ± 0.01	0.05 ± 0.01
4725......	2	−21.38 ± 0.13	0.70 ± 0.19	21.95 ± 0.13	8.96 ± 0.07	212.1 ± 5.4	3.75 ± 0.00	0.08 ± 0.05
4731......	6	−21.19 ± 0.15	0.41 ± 0.21	22.40 ± 0.15	10.08 ± 0.11	145.2 ± 0.8	3.18 ± 0.03	0.27 ± 0.04
4754......	−3	−20.68 ± 0.14	0.90 ± 0.11	19.58 ± 0.18	2.17 ± 0.11	42.148 ± 1.8	4.22 ± 0.02	0.00 ± 0.02
4861......	9	−19.52 ± 0.23	...	23.66 ± 0.23	8.37 ± 0.08	110.7 ± 1.2	3.58 ± 0.04	0.14 ± 0.07
4866......	−1	−20.17 ± 0.10	0.90 ± 0.14	20.35 ± 0.10	2.46 ± 0.03	62.7 ± 0.6	3.91 ± 0.03	0.04 ± 0.03
5005......	4	−21.86 ± 0.10	0.80 ± 0.11	20.57 ± 0.11	5.92 ± 0.15	96.7 ± 0.4	3.91 ± 0.01	0.20 ± 0.01
5033......	5	−21.54 ± 0.10	0.55 ± 0.15	22.04 ± 0.11	10.05 ± 0.12	166.2 ± 1.4	4.69 ± 0.02	0.18 ± 0.05
5055......	4	−20.78 ± 0.10	0.72 ± 0.14	21.14 ± 0.10	4.69 ± 0.05	216.5 ± 0.6	3.45 ± 0.00	0.19 ± 0.02
5204......	9	−17.58 ± 0.14	0.41 ± 0.18	21.79 ± 0.15	1.45 ± 0.04	90.5 ± 1.0	2.88 ± 0.07	0.25 ± 0.06
5248......	4	−21.82 ± 0.13	0.65 ± 0.18	21.34 ± 0.13	8.32 ± 0.08	103.6 ± 0.3	3.19 ± 0.02	0.20 ± 0.02
5322......	−5	−22.34 ± 0.16	0.89 ± 0.18	20.99 ± 0.18	8.97 ± 0.36	105.3 ± 3.2	4.87 ± 0.02	0.02 ± 0.01
5334......	5	−21.01 ± 0.22	...	23.41 ± 0.22	14.84 ± 0.23	126.3 ± 1.4	3.36 ± 0.04	0.09 ± 0.12
5364......	4	−21.84 ± 0.22	0.61 ± 0.18	22.29 ± 0.29	12.97 ± 1.09	161.5 ± 0.7	2.97 ± 0.01	0.15 ± 0.02
5371......	4	−22.45 ± 0.14	0.68 ± 0.20	21.64 ± 0.14	12.73 ± 0.06	105.7 ± 0.2	2.61 ± 0.02	0.14 ± 0.02
5377......	1	−21.14 ± 0.18	0.89 ± 0.18	21.38 ± 0.21	6.18 ± 0.34	76.2 ± 0.9	4.32 ± 0.03	0.07 ± 0.02
5585......	7	−18.79 ± 0.14	0.46 ± 0.20	21.97 ± 0.15	2.74 ± 0.05	135.8 ± 0.5	2.80 ± 0.02	0.16 ± 0.03
5669......	6	−20.85 ± 0.21	...	21.61 ± 0.21	6.00 ± 0.06	84.8 ± 0.5	2.74 ± 0.04	0.19 ± 0.06
5701......	0	−21.30 ± 0.14	0.84 ± 0.20	20.73 ± 0.14	4.91 ± 0.04	52.1 ± 0.3	4.28 ± 0.01	0.05 ± 0.02
5792......	3	−21.35 ± 0.13	0.78 ± 0.18	22.19 ± 0.13	9.85 ± 0.11	90.1 ± 0.7	3.32 ± 0.02	0.36 ± 0.03
5813......	−5	−21.74 ± 0.15	0.94 ± 0.18	21.02 ± 0.17	6.89 ± 0.24	83.4 ± 0.9	4.07 ± 0.03	0.03 ± 0.02
5850......	3	−21.68 ± 0.13	0.74 ± 0.18	21.54 ± 0.13	8.51 ± 0.09	109.2 ± 1.5	3.99 ± 0.04	0.08 ± 0.03
5985......	3	−22.09 ± 0.13	0.74 ± 0.18	22.20 ± 0.13	13.99 ± 0.06	107.1 ± 0.5	2.71 ± 0.01	0.11 ± 0.02
6015......	6	−20.45 ± 0.10	0.56 ± 0.14	21.76 ± 0.11	5.34 ± 0.07	91.4 ± 0.4	2.70 ± 0.01	0.19 ± 0.02
6118......	6	−21.10 ± 0.13	0.64 ± 0.18	22.38 ± 0.13	9.62 ± 0.10	112.8 ± 0.7	2.78 ± 0.03	0.14 ± 0.04
6384......	4	−22.14 ± 0.14	0.61 ± 0.20	21.42 ± 0.14	9.95 ± 0.06	138.5 ± 0.5	3.27 ± 0.02	0.13 ± 0.02

NOTE.—Col. (1): galaxy identification. Col. (2): morphological type of the galaxy. Col. (3): absolute B-band magnitude. Col. (4): rest-frame $B-V$ color. Col. (5): average surface brightness within the half-light radius. Col. (6): half-light radius (in kpc). Col. (7): radius corresponding to $\eta = 0.2$ (in arcseconds). Col. (8): image concentration. Col. (9): image asymmetry. Quantities in columns (5)–(9) are for the observed B_J or g bands.

3.1. *Photometric Parameters: Rest-Frame Color and Luminosity*

While the Frei et al. (1996) data set contains B_J images for 75% of the sample and g-band images for the remaining objects, there is no blue bandpass in which observations are available for all galaxies (see Table 1). We have made a comparison of the apparent (uncorrected) B magnitudes listed in the Third Reference Catalogue of Bright Galaxies (de Vaucouleurs et al. 1991, hereafter RC3) with those derived from our photometry of the Frei et al. images, appropriately transformed to the B band using the tabulated corrections of Frei & Gunn (1994). This comparison shows that, while the two magnitude estimates do not differ in the mean, there is a 0.25 mag (rms) scatter. To avoid the uncertainty associated with SED-dependent color transformations (see also § A.3) we use the RC3 uncorrected B magnitudes and $B-V$ colors, instead of the values from our own photometry.

We apply k-corrections and corrections for Galactic extinction to the $B-V$ colors and apparent B-band magnitudes of the nearby galaxy sample in the manner described in RC3. The heliocentric velocities $v_{\rm hc}$ of the galaxies are small (no greater than 3000 km s^{-1} for any object); the average velocity is $\langle v_{\rm hc} \rangle \sim 1000$ km s^{-1}. Hence the associated k-corrections are <0.05 mag. We use the distances given in the Nearby Galaxies Catalogue (Tully 1988), recalculated to $H_0 = 50$ km s^{-1} Mpc^{-1}, to derive absolute magnitudes M_B from the corrected apparent magnitudes. Note we do not correct for internal extinction since the suitability and procedure for applying such corrections may be ill defined for higher redshift galaxies.

3.2. *Multiaperture Photometry*

To characterize the light distributions of the galaxies, we performed multiaperture photometry on all images. The apertures are centered at the intensity-weighted centroid of each object. Since much of the profile shape information is contained in the central parts of the image, logarithmically spaced apertures are used. For the photometry of the *Hubble Space Telescope* (*HST*) images in Paper II, the smallest aperture corresponds to 0″.05, the largest to 15″; for the nearby galaxy photometry here, the aperture radii are scaled to correspond to similar linear sizes. The apertures are circular to accommodate the irregular morphology of the intermediate redshift galaxies in Paper II that would be difficult to fit with another geometrical figure. The efficacy of this approach is addressed in more detail below and in the Appendix (§ A.3).

3.3. *Structural Parameters*

Image structure is most commonly quantified via bulge–disk decomposition, yielding a bulge-to-total ratio B/T. We refrain from this approach here, for reasons we alluded to in the introduction. For example, B/T parameter may be poorly defined for asymmetric and compact galaxies. Irregularities in the surface brightness profiles, which can be caused by asymmetric structure, rings, or lenses, also cause problems for bulge–disk decompositions. While Kent showed that the concentration parameter correlates well with the bulge-to-total ratio, this holds only for objects with $B/T < 0.63$. At larger values of B/T, bulge-disk decomposition fails for several objects in Kent's sample, resulting in galaxies of type S0–Sa being given extremely high values of B/T. Bulge–disk decomposition also becomes unreliable when galaxy disks are fainter than the bulges.

It is worth noting again that these problems mainly arise from older, one-dimensional methods of decomposition. The newer two-dimensional decomposition techniques are clearly successful at reproducing the observed light profiles with remarkably small residuals (Schade et al. 1995, 1996; Simard 1998; Marleau & Simard 1998). Still, there are physical situations where bulge–disk decomposition techniques in general become problematic, namely, where the astrophysical reality is more complex than simple bulge–disk models. Some galaxies have central condensations better described by an exponential profile rather than an $r^{1/4}$ law (Wyse et al. 1997); many galaxies have strong bisymmetries, such as bars; virtually all galaxies have varying degrees of asymmetry due to star formation, dust, or large-scale gravitational perturbations and lopsidedness. All of these features represent details that decomposition into bulge and disk components do not address correctly. Simple disk and bulge decomposition is also inadequate for disk galaxies where the luminosity profile deviates from a pure exponential (Freeman 1970); e.g., type I and type II disks. (Type I disk profiles have an added component which contributes to the light just outside the bulge region; the surface brightness of a type II profile shows the opposite behavior [an inner truncation], and drops below the level of an exponential profile in the region near the center.)

Given the astrophysical complexity of real galaxies, the physical interpretation of the derived model parameters of disk-bulge fits remains uncertain. Nonetheless, such profile-fitting methods should be useful for estimating nonparametric structural and photometric parameters (e.g., characteristic sizes, surface brightness, image concentration, and ellipticity) in a way that uses the data in an optimal manner. In the current effort, however, we have taken a completely nonparametric approach of measuring sizes, surface brightness, image concentration, and asymmetry using multiaperture photometry, rather than deriving a model-dependent B/T parameter.

3.3.1. *Half-Light Radii and Surface Brightness*

We define first our working definition of a total magnitude, since it represents the critical zero point for measurement of the half-light radius and surface brightness. We use the dimensionless parameter η to define the total aperture of the galaxies—a limiting radius which is *not* based on isophotes.[2] The concept of defining the size of a galaxy based on the rate of change in the enclosed light as a function of radius was first introduced by Petrosian (1976). In terms of intensity, η can be defined as the ratio of the average surface brightness within radius r to the local surface brightness at r (Djorgovski & Spinrad 1981; Sandage & Perelmuter 1990). Like Wirth et al. (1994), we follow Kron's (1995) suggestion to use the inverted form $\eta(r) \equiv I(r)/\langle I(r)\rangle$, which equals one at the center of the galaxy and approaches zero at large galactic radii. The radius $r(\eta = 0.5)$ corresponds roughly to the half-light radius r_e.

Since η is defined as an intensity *ratio*, it is not affected by the surface brightness dimming effect that makes the use of isophotes problematic. Moreover, η is only dependent on the surface brightness within a given radius and not on any prior knowledge of total luminosity or the shape of the light profile. These properties make it advantageous for faint object photometry. We defined the "total" aperture of the intermediate-redshift objects as twice the radius $r(\eta = 0.2)$. The apparent total magnitudes are then defined within this aperture. For ideal Gaussian or exponential profiles, the magnitude $m_{0.2}$ within the radius $2r(\eta = 0.2)$ is approximately equal to the true total magnitude m_{tot}; more than 99% of the light is included within the radius $r(\eta = 0.2)$. For an $r^{1/4}$ law profile, there is a difference $m_{0.2} - m_{\text{tot}} \sim 0.13$ mag; this is due to the slow decline in luminosity at large radii that characterizes this profile. The radius $r(\eta = 0.2)$ was chosen based on visual inspection of the curves of growth derived from the aperture photometry out to large radii.

For reference, the theoretical value for the ratio of $r(\eta = 0.2)$ to half-light radius is 2.16, 1.95, and 1.82 for three standard profiles: exponential, Gaussian, and $r^{1/4}$ law, respectively. The observed ratio is 2.3 ± 0.3 for $B-V < 0.85$ (with little trend with color), but it rises slightly (2.6 ± 0.25) for the reddest galaxies with $B-V > 0.85$. A contributing cause to this rise is that for about half of the reddest objects, $r_{1/2}$ has been underestimated by $\sim 20\%$ because of their higher ellipticity. As we show in the Appendix (§ A.3.2), the half-light radii of early-type galaxies with axis ratio $a/b > 2$ are systematically underestimated by up to 30%. This effect will also cause small changes to the measured image concentration (§ 3.3.2) of these galaxies.

Finally, the angular half-light radii r_e were determined from the normalized curves of growth. Based on M_B and (corrected) R_e we calculated the photometric-structural parameter SB_e, the average blue surface brightness within the half-light radius, for all objects. For the nearby galaxy sample, the Tully catalog distances (as described in § 3.1) were used to determine R_e (kpc).

3.3.2. *Image Concentration*

We use the image concentration parameter C as defined by Kent (1985), which is based on the curve of growth. This parameter was shown to be closely correlated with Hubble

---

[2] Isophotal radii introduce redshift-dependent biases unless careful consideration and corrections are made for dimming due to the expansion [$\propto (1 + z)^{-3}$ in broadband photon counts] and k-corrections. While such redshift-dependent biases are not an issue for the samples studied in this paper, in future papers in the series this would be an issue were we not to avoid isophotes.

type for "normal" galaxies

$$C \equiv 5 \log(r_o/r_i) .$$

In the above equation, r_o and r_i are the outer and inner radii, enclosing some fraction of the total flux. In contrast, the concentration parameter defined by Abraham et al. (1994) is not based on curve of growth radii, but on a flux ratio within two isophotal radii.

However, in practice Kent also uses isophotes: He replaces the outer radius r_o, which encloses 80% of the total light, by the radius of the 24th mag arcsec^{-2} isophote. He has demonstrated that this radius encloses $\sim$79% of the total light for all galaxy types in the restrictive confines of his sample (Kent 1984). Because of the surface brightness dimming effect that becomes important for nonlocal galaxies, we instead use a method that is independent of isophotes. The total aperture of the galaxy, which determines the curve of growth, is defined based on the η-radius as described in § 3.3.1.

We have also explored the possibility of using η-radii to define a concentration parameter. However, a concentration parameter based on the curve of growth was ultimately found to be the more robust measure: the curve of growth increases monotonically with galactic radius for all objects, while the $\eta(r)$ function will be nonmonotonic for a "bumpy" light profile (like that of a well-resolved spiral galaxy). As a consequence, image concentration defined by the curve of growth rather than η exhibits less scatter when plotted against other correlated observables (e.g., color, surface brightness) than an image concentration parameter based on the η-function.

Anticipating our need to measure image concentration for small galaxies in Paper II and future papers in this series, we have studied the effects of spatial resolution and S/N on C. Here we focus primarily on resolution, as this was the dominant effect. The importance of resolution is demonstrated by the comparison of Schade et al. (1996) of decompositions of compact objects in ground-based and *HST* images: the cores of the blue nucleated galaxies are not resolved in ground-based imaging, and hence they are frequently misclassified as having much lower B/T ratios than what is revealed by *HST* imaging. In Paper II we analyze this sample of galaxies, and hence this illustration is of particular relevance.

Resolution effects on image concentration were estimated by block-averaging the images of nearby galaxy sample over a range of values until the spatial sampling (as measured in pixels per half-light radius) was comparable to that of the compact galaxies at intermediate redshift observed with the *HST* Wide Field Planetary Camera 2 (WFPC2). The details of these simulations are presented in the Appendix (§ A.1). In short, as the objects' half-light radii get smaller, the scatter in the measured concentration indices increases. While larger inner radii or a smaller outer radii decrease this scatter (because of improved resolution and S/N, respectively), such choices decrease the dynamic range of the concentration index.

Based on these simulations, we chose a definition of C that is, to first order, sufficiently robust to allow a direct comparison of the image concentration of the local and the higher redshift samples studied here and in Paper II and, furthermore, gives a large dynamic range: $C = 5 \log [r(80\%)/r(20\%)]$. This concentration index is remarkably stable: the mean concentration does not deviate from that measured in the original image by more than 0.2, or $\sim$8% of the dynamic range in C, down to resolution of 5 pixels per half-light radius.

Our definition is sufficiently close to that of Kent (1985) so that it is meaningful to compare our values directly with those he determined from photometric analysis of a sample of nearby galaxies. With this choice of radii, a theoretical $r^{1/4}$-law profile has $C = 5.2$, an exponential profile has $C = 2.7$, and a Gaussian has $C = 2.1$. These values agree well with the results of Kent's analysis: he finds that elliptical galaxies have $C \sim 5.2$, and late-type spirals have $C \sim 3.3$.

Lastly, since we use circular apertures, the measured image concentration may be affected by the ellipticity of the galaxy. Based on the comparison between our results for the Frei et al. sample and those of Kent's elliptical aperture photometry, we believe this to be a negligible effect in all cases but the earliest, must elliptic galaxies. Wirth et al. (1994) found that for an $r^{1/4}$ law profile with axis ratio $b/a = 0.2$, the change in C is less than 5%. The effect appears to be larger in our study. A more detailed description of this possible systematic is given in the Appendix.

3.3.3. *Image Asymmetry*

The last image structure parameter is rotational asymmetry A, as defined by Conselice et a. (2000). This definition differs from earlier methods in that the asymmetry is determined within a constant η-radius of $\eta = 0.2$, a noise correction is applied, and an iterative procedure which minimizes A is used to define the center of rotation. This algorithm was tested to be robust to changes in spatial resolution and signal-to-noise by Conselice et al. (2000) using simulations similar to those described here for the concentration parameter C; the systematics with resolution are below 10% of the original value for galaxies in this paper and in Paper II.

3.3.4. *Morphological K-Corrections*

To obviate the issue of "morphological" k-corrections, image structural parameters should ideally be measured at the same rest-frame wavelength for all objects. Anticipating our needs to derive the structural parameters for intermediate-redshift objects in Paper II (and future papers in this series), we have adopted the following protocol: (1) For the nearby galaxy sample we use the images in the B_J and g bands to derive the primary local image structure parameters. (The rest-frame wavelengths sampled by the R,r–band images correspond to bands redshifted into the near-infrared for the intermediate-redshift galaxies.) (2) We use the multiband images of the Frei et al. sample to determine corrections to compensate for the wavelength dependence of asymmetry, concentration, and half-light radius—as described in the Appendix (§ A.2). For example, WFPC2 images in the I_{814} band of objects between $0.3 < z < 0.8$ correspond to first order to the rest-wavelength range of the B_J and g bands. Nonetheless, the effective rest-wavelength for such intermediate-redshift galaxies is typically slightly redward of rest frame B_J and g bands. The corrections in § A.2 are suitable for such samples, as well as higher redshift samples imaged in redder bands.

4. RESULTS

4.1. *Mean Properties, Distributions, and Correlations*

The mean properties for our six parameters (M_B, $B-V$, R_e, SB$_e$, C, and A) are listed in Table 3 as a function of

TABLE 3

AVERAGE GALAXY PROPERTIES

Type (1)	Sample (2)	M_B (3)	$B-V$ (4)	R_e (5)	SB_e (6)	C (7)	A (8)
E–S0	Frei	$-21.4^{+1.2}_{-0.4}$	$0.9^{+0.0}_{-0.0}$	$4.6^{+2.2}_{-2.3}$	$20.3^{+0.7}_{-0.4}$	$4.2^{+0.2}_{-0.2}$	$0.03^{+0.01}_{-0.02}$
Sa–Sb	Frei	$-21.5^{+0.6}_{-0.3}$	$0.7^{+0.1}_{-0.1}$	$8.3^{+1.6}_{-3.4}$	$21.3^{+0.8}_{-0.2}$	$3.5^{+0.4}_{-0.5}$	$0.13^{+0.03}_{-0.06}$
Sc–Irr	Frei	$-20.6^{+1.2}_{-0.4}$	$0.6^{+0.1}_{-0.1}$	$6.4^{+1.1}_{-2.4}$	$21.7^{+0.6}_{-0.2}$	$3.0^{+0.3}_{-0.3}$	$0.17^{+0.07}_{-0.04}$
E–S0	Kent	$-20.8^{+0.4}_{-0.2}$	$0.9^{+0.0}_{-0.0}$	...	...	$5.0^{+0.3}_{-0.3}$	...
Sa–Sb	Kent	$-21.0^{+0.4}_{-0.2}$	$0.8^{+0.1}_{-0.1}$	...	...	$4.2^{+0.5}_{-0.5}$	...
Sc–Irr	Kent	$-20.9^{+0.4}_{-0.1}$	$0.6^{+0.1}_{-0.1}$	...	...	$3.4^{+0.4}_{-0.6}$	...
E–S0	Huchra	$-20.5^{+2.7}_{-0.4}$	$0.7^{+0.1}_{-0.0}$	...	...	...	...
Sa–Sb	Huchra	$-21.0^{+1.6}_{-0.4}$	$0.7^{+0.1}_{-0.0}$	...	...	...	...
Sc–Irr	Huchra	$-21.0^{+1.8}_{-0.4}$	$0.5^{+0.1}_{-0.1}$	...	...	...	...

NOTE.—Col. (1): Hubble type of the objects. Col. (2): code representing the sample from which each source was extracted: Frei et al. (1996), Kent (1984), or Huchra (1977a). Cols. (3)–(8): same as columns (3)–(6) and (8)–(9) in Table 2. Structural parameters are corrected to correspond to the rest-frame *B* band, except for Kent's sample where *r*-band image concentration is listed. For all columns, the middle 50% of the sample is contained within the listed bounds.

Hubble type. While we would like to move away from using Hubble types, they are so ingrained in the astronomical culture that they are a useful point of departure. For clarity in the following discussion, we group these types together into early (E–S0), intermediate (Sa–Sb), and late (Sc–Irr). These names are potentially misleading, of course, and so we encourage the reader to treat them as labels that, at best, evoke a well-conceived galaxy type but not necessarily an evolutionary state. Clearly further subdivision could be made, but our current purposes are illustrative, not definitive.

A typical approach to exploring the correlations in (and dimensionality of) a multivariate parameter space is principal component analysis. While this is valuable, it is not particularly instructive for a first understanding of the distribution of different types of objects in the parameter space. We are interested both in correlations between observables and in trends as a function of the qualitative Hubble type. These correlations and trends need not be one and the same. For example, two observables can be uncorrelated but still exhibit a distribution segregated by Hubble type. To develop such an understanding, we therefore inspected the 15 possible two-dimensional projections of our six-dimensional parameter space.

To distill this information further, we considered that there are in fact three types of physically distinct parameters:

1. Spectral index (color): this parameter is purely photometric, by which we mean there is no information about the shape of the light profile. There is also no scale information; i.e., the amplitude and size of the light profile is also unimportant. In the balance of this paper we will use "color" and "spectral index" interchangeably.

2. Form (A, C): these parameters are purely structural, by which we mean that they do not depend—to first order—on the amplitude or the shape of the spectral energy distribution, nor on the physical scale of the light distribution; they reflect only the *shape* of the light profile.[3]

3. Scale (R_e, L, and SB_e): these parameters are physically distinct. Luminosity is purely photometric (by our above definition). Size, which we also refer to as a structural parameter, is influenced by image shape, i.e., depending on the definition of size, two galaxies with different light profile *shapes* can have relatively different *sizes* (see § 3.3.1, for example). Surface brightness is a hybrid, photometric *and* structural, parameter; it is a function of size and luminosity. While surface brightness is a ratio of luminosity to surface area, it is still a measure of "scale"—in this case, the luminosity surface density.[4]

This reduces the types of combinations (by parameter type) to six, i.e., between color, form, and scale.

We find the strongest and physically most interesting correlations are between color, form, and the one scale parameter, SB_e (Figs. 3–5). We focus on these for the remainder of the paper. Before turning to them, for completeness we first summarize our observations of the other types of correlations.

Color-color correlations are strong and well known (e.g., Fig. 2). Effectively they add higher order information about spectral type. Here we consider only $B-V$ as a simple spectral index that effectively represents the first-order information of spectral type. In general, one might adopt several spectral indices, e.g., $U-V$ and $V-K$, or a single index based on multicolors.

Color-scale correlations also have been explored in detail elsewhere; e.g., color-luminosity relationships, known to exist for all galaxy types in both the optical and near-infrared (Huchra 1977b; Mobasher et al. 1986; Bershady 1995). The limited dynamic range of the Frei et al. sample in size and luminosity (they are mostly large and luminous systems) preclude useful results being drawn here in this regard. For example, the correlation of color with size in this sample is subtle and depends in detail on how size is defined, as noted above. Form-scale correlations including size and luminosity are also difficult to assess for this sample for the same reasons of limited dynamic range in scale. However, scale versus scale *is* an interesting diagnostic, because, for example, size and luminosity allow one to probe the range of surface brightness in the sample. We explore this in Paper II.

---

[3] We consider image concentration to be a form, in contrast to Morgan who used it as a surrogate for spectral index.

[4] A fourth scale parameter that we do not consider here is line width, or some measure of the amplitude of the internal dynamics.

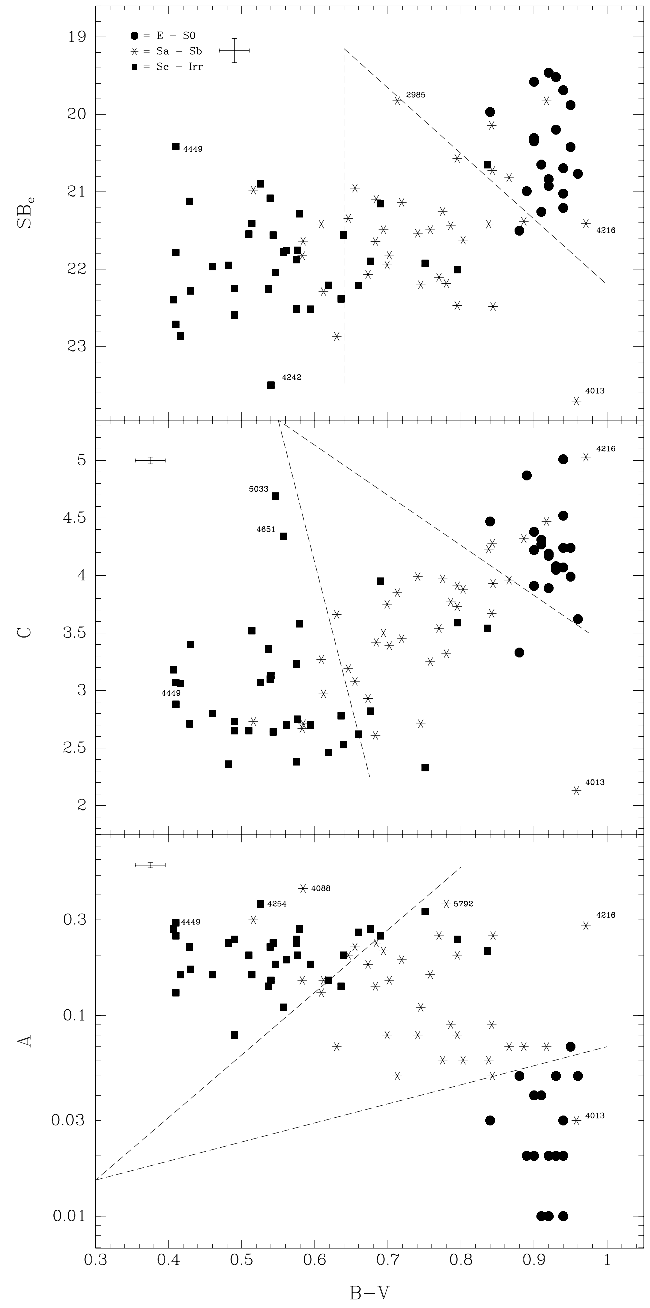

FIG. 3.—Rest-frame *B*-band form and scale parameters vs. spectral index for the Frei et al. sample. *Top*: Average surface-brightness within the half-light radius (SB$_e$) vs. rest-frame $B-V$. *Middle*: Image concentration (C) vs. $B-V$. *Bottom*: 180° rotational image asymmetry (A) vs. $B-V$. Characteristic errors are given in the top left corner of each panel. Outlying objects are labeled and discussed in the text. Dashed lines demark early, intermediate, and late types in our classification scheme. Symbols are by Hubble type, as defined in the key. Different Hubble types are well distinguished, particularly in color. Morphological types are also well separated in C, but only the earliest types are well separated in SB$_e$ and A.

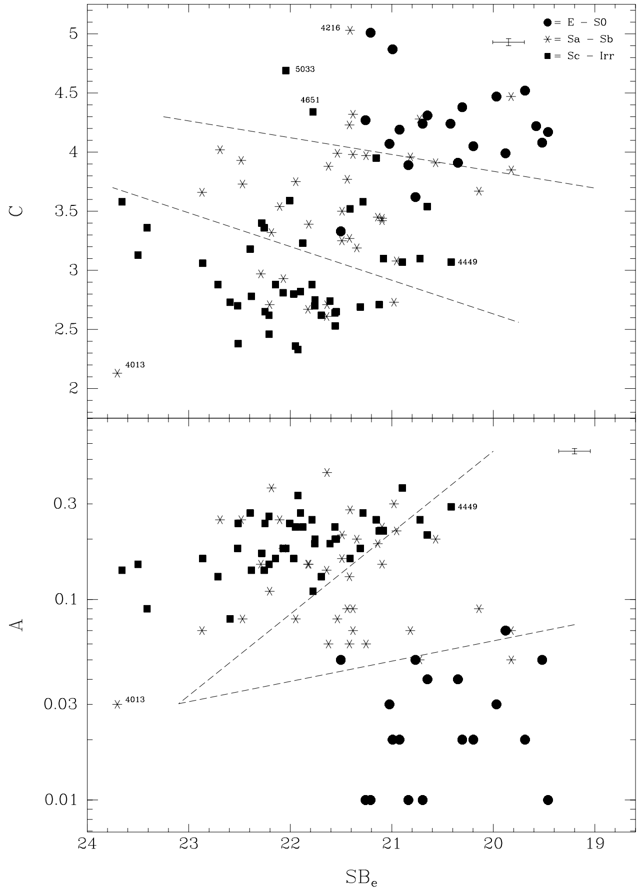

FIG. 4.—Rest-frame *B*-band parameters of form vs. scale for the Frei et al. sample. *Top*: Image asymmetry (A) vs. average surface-brightness (SB$_e$). Bottom panel: image concentration (C) versus SB$_e$. Outlying objects are labeled and discussed in the text. Dashed lines demark early, intermediate, and late types in our classification scheme. The separation of morphological types is less clear than in Fig. 3, but the different Hubble types are still reasonably segregated.

4.1.1. *Spectral Index versus Form and Scale*

Strong correlations exist in all three plots of color versus form parameters C and A and scale parameter SB$_e$ (Fig. 3). Early-type galaxies are redder, more concentrated, high surface brightness, and more symmetric than intermediate- and late-type systems. The best correlation is between color and concentration in the sense that there is a smooth change in both quantities with Hubble type. This is expected from a simple interpretation of the Hubble sequence as a sequence parameterized by the relative dominance of a red, concentrated bulge (or spheroid) versus a bluer, more diffuse disk.[5] In contrast, the distinction between Hubble types in SB$_e$ and A is most pronounced between early types and the remainder; intermediate- and late-type galaxies are not well distinguished by either of these parameters.

A more complete local sample will likely include a larger fraction of objects that do not follow these trends. For example, amorphous galaxies have surface brightnesses comparable to elliptical galaxies but are generally quite blue in color (Gallagher & Hunter 1987; Marlowe et al. 1997). Nonetheless, what is physically compelling about these color-form correlations is that each axis carries dis-

---

[5] A few of the local galaxies have values of C that are lower than the theoretical concentration for an exponential disk (the errors in C are $\lesssim 0.02$ for all of them). The majority of these objects are late-type spiral galaxies with prominent, bright regions of star formation in the spiral arms. The star-forming regions cause the image profiles to become less centrally concentrated than a simple disk profile.

tinct information, respectively, on the integrated stellar population and its spatial distribution.

4.1.2. *Form versus Form and Scale*

There are clear trends present in the two plots of form versus SB_e (scale) in Figure 4, as well as the plot of form parameters alone in Figure 5. More centrally concentrated galaxies have higher average surface brightnesses and lower asymmetry; more symmetric objects have higher surface brightness. In general, the concentrated, high surface brightness galaxies are early type, while the late-type galaxies are less concentrated, have lower surface brightness, and are more asymmetric. While there is substantial scatter in the form and scale parameters for early and late types, these two extreme groups still are well separated in the above three plots. The intermediate-type galaxies, however, are *not* well separated from these extremes, and they tend to overlap substantially with the late-type galaxies, consistent with what is found in plots of color versus form and scale: intermediate- and late-type galaxies have comparable degrees of asymmetry and similar surface brightness.

One should be cautious in concluding the relative merits of form-scale and form-form versus color-form and color-scale correlations based on the relative separation of Hubble types. Using Hubble types may be unfair if, for example, they were designed to correlate well with color but not necessarily with the quantitative form and scale parameters explored here. Since the form-form and form-scale correlations themselves are comparable, and nearly as strong as for color-form and color-scale, we are inclined to consider both as part of a general classification scheme. Certainly the form and scale parameters will each have different sensitivity to stellar evolution than color and so are advantageous to consider in isolation.

4.1.3. *Comparisons with Previous Work*

The correlation between image concentration and mean surface brightness within the effective radius (Fig. 4) has been explored by several groups in the context of galaxy classification (Okamura et al. 1984; Watanabe et al. 1985; Doi et al. 1993; Abraham et al. 1994). We focus here, however, on Kent's (1985) *r*-band study, since his definition of image concentration and effective surface brightness are the most similar to our own. While similar, the slope of the correlation is nonetheless steeper for our sample, albeit with much larger scatter, as illustrated in the top panel of Figure 6. As the middle and bottom panels reveal, the cause of the steeper slope in our sample is the smaller dynamic range in image concentration. This is likely due to the fact that we use circular apertures when performing surface photometry, whereas Kent used elliptical apertures. We attempt to quantify the systematics due to differences in aperture shape in § A.3. While the dynamic range in image concentration is reduced using circular apertures for the Frei et al. sample, there does appear to be a somewhat smaller scatter in C as a function of $B-V$.

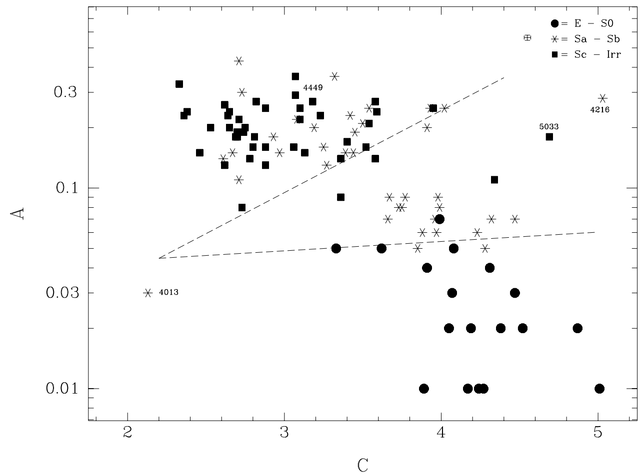

FIG. 5.—Form vs. form parameters for the Frei et al. sample: rest-frame B-band image asymmetry (A) vs. image concentration (C). Outlying objects are labeled and discussed in the text. Dashed lines demark early, intermediate, and late types in our classification scheme. The separation of morphological types is less clear than in Fig. 3, but is comparable with Fig. 4, where the different Hubble types are reasonably segregated.

The nature of the large scatter in the top two panels of Figure 6 for the Frei et al. sample is also discussed further in § A.3. In short, we believe much of this scatter is due to uncertainties in the R- and r-band zero points of the Frei et al. sample. These uncertainties adversely affect only the surface brightness values in Figure 6. Robust estimators of the scatter about a mean regression (i.e., iterative sigma clipping of outlying points) eliminate the outlying points, but still yield 50% larger scatter in R-band SB_e for the Frei et al. sample as a function of either image concentration or $B-V$. A plausible additional source contributing to this larger scatter is that Kent's observed surface brightnesses were converted to face-on values, while ours were not "corrected" in this way. We conclude that if it is possible to apply accurate and appropriate inclination corrections to all galaxies in a given study, this would be desirable. Since such corrections cannot be performed for the intermediate-redshift objects in Paper II (and in general, if such corrections are not possible for a critical subset of the data), we believe it is best not make such corrections at *any* redshift.

The asymmetry-concentration plane has also been explored for galaxy classification purposes by, e.g., Abraham et al. (1994, 1996a) and Brinchmann et al. (1998). Our methods of measuring these parameters differ from theirs, and thus our quantitative results cannot be directly compared. However, a qualitative comparison to the $A-C$ plot of Brinchmann et al. shows that both methods yield very similar results: the distribution of galaxies can be subdivided into sectors where early-type, intermediate-type, and late-type objects dominate. Brinchmann et al. also use the local sample from the Frei catalog to define these bins, but note however that the points they plot represent a sample of intermediate-redshift galaxies. The $A-C$ correlation in the Brinchmann et al. diagram is not as clear as that seen here for the local sample in Figure 5; the scatter in their diagram is comparable to the dynamic range of the parameters. This is probably due to the different properties of the samples, rather than to the differences in how we determine the parameters. For a more direct comparison, we plot B band asymmetry and concentration versus rest-frame $B-V$ color for 70 galaxies from the Frei et al. sample (Fig. 7), using both the A, C values from this study and those found by Brinchmann et al. It can be seen that the distributions are overall quite similar; however, the separation in asymmetry of the different Hubble types is more apparent in this study, and the scatter in concentration is somewhat smaller. The conclusion here, then, is that our methodology offers typically modest, but sometimes significant, improvements over previous work.

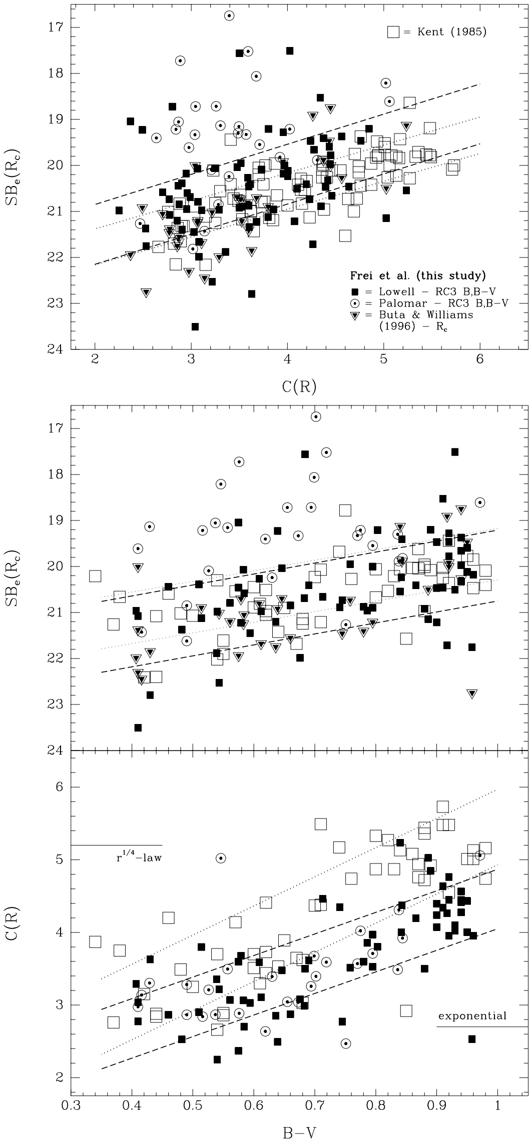

FIG. 6.—Comparison of form, scale, and spectral index correlations between Frei et al. and Kent samples. *Top panel:* Average *R*-band (Kron-Cousins) surface brightness within the half-light radius $SB_e(R_c)$ vs. *R*- or *r*-band image concentration *C*(*R*). *Middle*: $SB_e(R_c)$ vs. rest-frame $B-V$. *Bottom*: *C*(*R*) vs. rest-frame $B-V$. Structural parameters: We have measured half-light radius and image concentration for the Frei et al. sample using their *R*- or *r*-band CCD images and circular photometry apertures. Kent measured these structural parameters using elliptical apertures on *F*-band CCD images. Photometric parameters: The Frei et al. sample is subdivided between objects observed at (1) Lowell Observatory (*filled squares*), (2) Palomar Observatory (*dotted circles*), and (3) an overlapping subset of the Frei et al. sample with existing R_c-band photometry from Buta & Williams (1996; *outlined triangles*). For (1) and (2) we used the zero points from the Frei et al. image headers (DNATO_BV) and transformations from Thuan-Gunn *r* and Gullixson et al. *R* to Cousins R_c from Frei & Gunn (1994). We have transformed Kent's photometry reported in the Thuan-Gunn *r*-band to R_c again based on transformations in Frei & Gunn (1994); Kent corrected surface brightnesses to "face-on" values. Regressions: Lines indicate $\pm 1\ \sigma$ about linear least-squares fits to the correlations (*dotted*, Kent; *dashed*, Frei et al.) using an iterative clipping method ($\pm 2.5\ \sigma$ clip, 10 iterations). In the top and middle panels only the Lowell subset of the Frei et al. sample was used in the regressions. The substantial scatter in the Frei et al. $SB_e(R_c)$ values we infer is due primarily to zero-point uncertainties; we detect no noticeable systematics effects with inclination in $SB_e(R_c)$. The difference in the correlation between $SB_e(R_c)$ and *C*(*R*) is largely due to the shallower trend in *C*(*R*) with $B-V$ for the Frei et al. sample. This may be due to differences between circular vs. elliptical apertures. While elliptical aperture photometry provides greater dynamic range in *C*(*R*), the correlation of *C*(*R*) with $B-V$ has larger scatter.

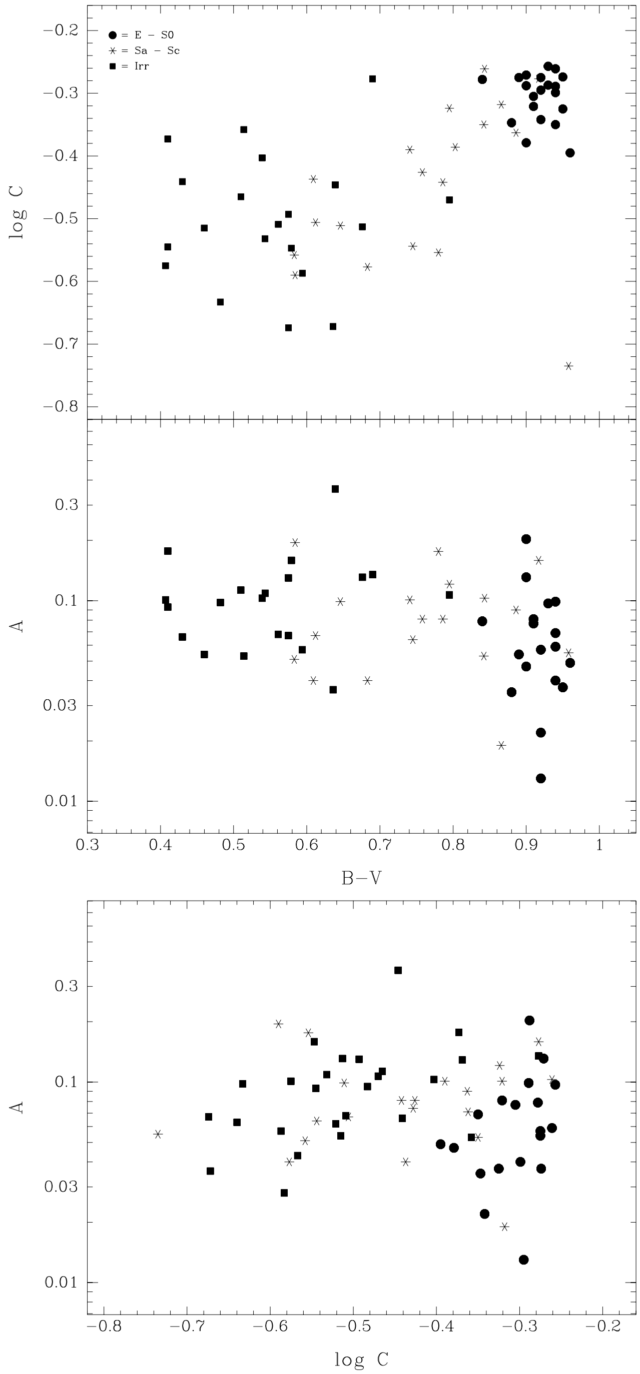

FIG. 7.—Form parameters and spectral index for 70 galaxies from the Frei et al. sample as determined by Brinchmann et al. *Top*: *B*-band image concentration vs. rest-frame $B-V$. *Middle*: *B*-band asymmetry versus rest-frame $B-V$. *Bottom*: *B*-band asymmetry versus concentration. The asymmetry parameter was determined in a very similar manner to our own and thus should have comparable dynamic range. Since our *C* parameter is logarithmic, we plot the logarithm of the Brinchmann et al. *C* values. These plots are displayed so that they may be directly compared with Figs. 3 and 5. The trend in asymmetry for the different Hubble types is more apparent in Figs. 3 and 5. In the concentration–color plane, the distributions are similar for both studies, although we find a smaller scatter among the late-type galaxies and a larger scatter among the early-type objects.

4.2. *Classification*

The above results point to how we can most effectively define a parameter demarcation to isolate, identify, and classify normal galaxies. In the four-dimensional parameter space of ($B-V$, A, SB_e, C), we define boundaries ("cuts") in the six two-dimensional projections between galaxies classified in the Hubble sequence as early/intermediate and intermediate/late. These boundaries, selected by eye on the basis of the distribution of Hubble types, are listed in Table 4 and illustrated in Figures 3–5. Segregation by higher dimensional hypersurfaces are likely to be more effective (galaxies appear to be distributed on a "fundamental" hypersurface—the subject of a future paper), but the projected boundaries here are meant to be illustrative, as well as practical for application when all of the parameters are not available. We stress that these boundaries are not definitive in some deeper physical sense. For example, in terms of formal Hubble types, cuts involving color are clearly "best"; however, as noted above, this may not be physically significant.

It would be uninteresting if all of the cuts provided the same classification. Moreover, one expects there will be discrepancies for objects near boundaries. We find that 49% of the sample matches in all cuts, while 64%, 87%, and 99% of the sample matches in at least five, four, or three cuts, respectively. (Hereafter, we refer to cases where five out of six cuts match as "5/6," etc.) This degree of consistency seems reasonable, so we have not tried to fine-tune the boundaries (such fine-tuning would not be sensible anyway since the details of the classification self-consistency are likely to be sample dependent). The preponderance of objects are classifiable by a simple majority of the classifications based on the six cuts; 13% of the objects have a more ambiguous classification.

Of interest are the discrepancies within and between cuts in different combinations of color, form, and scale. We found that it is useful to group the six cuts into two groups of three. The first consists of the cuts in Figure 3 between color, form and scale, which we refer to as color-form/scale. The second consists of the cuts in Figures 4 and 5 between form and scale, which we refer to as scale/form-form. For example, 64% of the variance in the 5/6 cases comes from cuts in C–SB_e, whereas cuts in C–$(B-V)$ and A–C are always consistent with the majority classification. More generally, scale/form-form cuts are internally mismatched 40% of the time, while color-form/scale cuts are internally mismatched only 21% of the time (and two-thirds of these color-form/scale mismatches are also present in scale/form-form mismatches). In other words, the color-form/scale cuts tend to be more consistent; much of the variance in the scale/form-form cuts again comes from C–SB_e.

Only two galaxies pose a substantial problem for classification: NGC 4013 and NGC 4216. They are classified by various cuts to be in all categories (early, intermediate, and late) and have no majority classification. However, both are highly inclined (NGC 4013 is edge on), which appears to give them unusual observed properties. Indeed, they are extreme outliers in several of the projections in Figures 3 and 4 (see also § A.3.2 and figures therein). Hence such problem cases are likely to be easy to identify. Three other sources classified in all three categories (NGC 4414, 4651, and 5033) are not a problem: They have 4/6 consistent classifications. Two of these (NGC 4651 and NGC 5033) have Seyfert nuclei and are outliers only in plots with image concentration; they are highly concentrated for their color. NGC 4414 is not an outlier in any of the plots.

Finally, it is interesting to note that 23% of the sample has inconsistent majority classifications in color-form/scale versus scale/form-form cuts. This is true for 100% of the 3/6 cases and 55% of the 4/6 cases. However, we believe this is for different reasons. In the latter cases (only) we find that the galaxies are predominantly at high inclination (∼50% excess in the top half and top quartile of the sample distribution in inclination). Moreover, the color-form/scale classifications in these cases are all *earlier* than the majority scale/form-form classifications. We surmise this is due to the effects of reddening on $B-V$.[6] While the color-form/scale classifications tend to be earlier for the 3/6 cases, because there is no apparent inclination dependence, these differences are due likely to other physical effects. Two possibilities include low star formation rates or high metallicity for galaxies of their form. Both of these conjectures are testable via spectroscopic observation.

We suggest then, as a practical, *simple* prescription, that the majority classification for all six cuts be taken as the classifier, except in the situation where the galaxy in question is highly inclined. In the latter case, the majority classification of the scale/form-form cuts should be adopted. When galaxies have only 3/3 consistent classifications (13% of the Frei et al. sample), the adopted classifier should be intermediate between the two most common classifications. It also may be of interest to note if the color-form/scale and scale/form-form majority classifications differ. However, further elaboration based on these two-dimensional projec-

TABLE 4

CLASSIFICATION BOUNDARIES

Parameters (1)	Early/Intermediate (2)	Intermediate/Late (3)	Figure (4)
SB_e, $B-V$	$B-V = 0.12\ \mathrm{SB}_e - 1.66$	$B-V = 0.64$	3
C, $B-V$	$B-V = -0.23\ C + 1.78$	$B-V = -0.04\ C + 0.76$	3
A, $B-V$	$B-V = 1.05 \log A + 2.21$	$B-V = 0.32 \log A + 0.88$	3
C, SB_e	$\mathrm{SB}_e = 7.04\ C - 7.02$	$\mathrm{SB}_e = 3.52\ C + 10.73$	4
A, SB_e	$\mathrm{SB}_e = -10.4 \log A + 7.29$	$\mathrm{SB}_e = -2.46 \log A + 19.36$	4
A, C	$C = 21.5 \log A + 31.2$	$C = 2.44 \log A + 5.49$	5

NOTE.—Col. (1): parameter pair. Col. (2): boundary between early and intermediate-type galaxies. Col. (3): boundary between intermediate and late-type galaxies. Col. (4): corresponding figure in this paper.

---

[6] Inclination will also cause changes in other measured parameters. Changes in C, however, appear to be small (see § A.3.2). Surface brightness will tend to increase at modest inclinations and then decrease at high inclinations if a prominent dust lane obscures the bulge. Likewise, A may increase because of a dust lane until the galaxy is directly edge-on. As a consequence of these changes and the distributions and cuts, C–SB_e tends to mimic the color-form cuts in the high-inclination cases, while A–SB_e and A–C do not.

tions of a higher dimensional distribution is not likely to be warranted.

4.2.1. *Discussion*

We note that there are no distance-dependent scale parameters in our classification. By this we mean specifically that the classification parameters do not depend on knowledge of the distance modulus. Hence this classification is both quantitative and independent of the cosmological distance scale and its change with cosmological epoch (i.e., no a priori knowledge is needed about H_0 or q_0). The effects of the expansion do change the *observed* classification parameters. However, with knowledge of galaxy redshifts and judicious choice of "redshifted" photometric bands, surface brightness dimming can be corrected and band-shifting either eliminated or corrected via the protocol described in the Appendix. Galaxy evolution, of course, will also modify the values of the parameters, but this is precisely the utility of the classification systems as applied to such a study: In what way do the parameters and their correlations evolve? How do the scale parameters change for a fixed range in classification parameters? These are issues that we intend to explore in subsequent papers in this series.

We also comment on the efficacy of using the four-dimensional parameter space of color, concentration, surface-brightness, and asymmetry for the classification of distant galaxies. As noted earlier, Abraham et al. (1996a) and Brinchmann et al. (1998) have explored the use of the asymmetry–concentration plane as a tool for distant galaxy classification. The use of the additional parameters of color and surface-brightness are clearly advantageous; they offer substantially more information, particularly as a diagnostic of the stellar population age and surface density. The reasoning behind using A and C alone has been that to first order, they can be estimated without redshift information. Yet the wavelength dependence of both parameters (i.e., what is referred to as "morphological k-corrections") can lead to measurement systematics. These systematics, if not corrected, in turn result in objects over a range in redshift being systematically misclassified. For example, Brinchmann estimates that at $z = 0.9$, 25% of spiral galaxies are *misclassified* as peculiar objects in the $A-C$ plane. This fraction is expected to increase at larger redshifts. Hence, for high-z studies of galaxy morphology, redshift information is crucial even when using asymmetry and concentration. Therefore, since redshift information is crucial no matter what, there is no reason *not* to use the four-dimensional classification we have outlined in future studies. The recent refinements and calibration of the technique of estimating redshifts photometrically make this all the more tractable.

Finally, we note that while the classification we have proposed here is practical and useful, there are five areas where we anticipate it can be improved or elaborated. (1) As we have mentioned before, the spectral-index parameter could have much greater leverage in distinguishing between different stellar populations by adding passbands that expand the wavelength baseline (e.g., the U and K bands in the near-UV and near-IR, respectively) or by increasing the spectral resolution (e.g., line strengths and ratios). A further step of elaboration would be to explore spatially resolved spectral indices (gradients) and determine their correlation with form parameters. (2) Internal kinematics should be considered. Ideally, the kinematic information would include estimates of both the random and ordered motion (rotation) so that the dynamical temperature could be assessed, in addition to the overall scale. Kinematics are relatively expensive to obtain (compared with images), but with modern spectrographs on large telescopes, the absolute cost is minimal at least for nearby galaxies. (3) Higher dimensional correlations are worthy of exploration to determine, for example, whether "fundamental" hyperplanes can adequately describe the entirety of the galaxy distribution. (4) It is worth considering whether there are additional form parameters of value for classification that have not been included here. (5) The classification scheme needs to be tested against much larger and more volume-representative samples of galaxies.

5. SUMMARY AND CONCLUSIONS

We have presented results from a study of the photometric and image-structural characteristics and correlations of a sample of local, bright galaxies (Frei et al. 1996). We find it illuminating to distinguish between parameters that characterize spectral index (color), form (image concentration and asymmetry), and scale (size, luminosity, and surface brightness). In this context, we arrive at the following main results and conclusions.

1. We find that a combination of spectral index, form, and scale parameters has the greatest discriminatory power in separating normal Hubble types. The strongest correlation is found between color and image concentration. However, there are equally strong correlations between form parameters (e.g., A and C), but here the Hubble types are not as well distinguished. As an indicator of classification utility, we suggest that the strength of the correlation between parameters is likely more important than the separation of Hubble types within the correlation.
2. It is possible to define a quantitative classification system for normal galaxies based on a four-parameter subset of spectral index, form, and scale: rest-frame $B-V$ color, image concentration, asymmetry, and average surface brightness within the half-light radius. We propose a specific classification that distinguishes between "normal" galaxies as early, intermediate, and late based on cuts in these four parameters. The classification is successful for 99% of the Frei et al. sample. Nonetheless, we designate this as preliminary until larger, more comprehensive samples of galaxies are analyzed than in the present study.
3. Distance-dependent scale parameters are *not* part of this preliminary classification.
4. These classification parameters can be measured reliably over a broad range in S/N and image resolution, and hence they should be suitable for reliably distinguishing between a wide variety of galaxies over a large range in redshift.
5. Redshift information *is* needed to reliably estimate both the photometric properties (rest-frame color and surface brightness) as well as the structural parameters asymmetry and concentration at a fixed (B-band) rest-frame wavelength. In terms of redshift independence, asymmetry and concentration alone thus offer no advantages over the additional classifierss proposed here. Indeed, incorporating the full suite of parameters defined here is advantageous for the purposes of classification.

The authors wish to thank Greg Wirth for his highly refined algorithm for calculating η-radii used here and in

Paper II, our collaborators David Koo and Rafael Guzmán for their comments on the manuscript and input on assembling dwarf galaxy samples, and Jarle Brinchmann for providing us with his measurements of structural parameters for the local galaxy sample. We also gratefully acknowledge Jay Gallagher and Jane Charlton for a critical reading of the original version of this paper and Paper II, and for useful discussions of this work. Most importantly, we thank Zolt Frei, Puragra Guhathakurta, James Gunn, and Anthony Tyson for making their fine set of digital images publicly available. Funding for this work was provided by NASA grants AR-07519.01 and GO-7875 from Space Telescope Science Institute, which is operated by the Association of Universities for Research in Astronomy, under contract NAS 5-26555. Additional support came from NASA/LTSA grant NAG 5-6032.

APPENDIX

CORRECTIONS FOR MEASUREMENT SYSTEMATICS

Here we establish the measurement systematics due to changes in image resolution for half-light radius and image concentration and for band-shifting effects on half-light radius and image concentration and asymmetry. Systematic effects of image resolution and noise on asymmetry are quantified in Conselice et al. (2000).

A1. RESOLUTION DEPENDENCE OF OBSERVED SIZE AND IMAGE CONCENTRATION

To maximize the dynamic range of the measured concentration index C, the inner radius should be small and the outer radius large relative to the half-light radius. In this way, one samples the light profile gradients in both the central and outer regions of a galaxy where the bulge and disk contribute quite differently. This strategy maximizes the leverage for discriminating between different profiles, e.g., exponential and $r^{1/4}$ law. In the presence of noise and limited spatial resolution, however, the choice of radii determines the robustness of the concentration index. As noted by Kent (1985), the inner radius should be large enough to be relatively insensitive to seeing effects, and the outer radius should not be so large that it is affected by uncertainties in the sky background and S/N. In the current study, the sources are resolved and the images are at moderately high signal to noise: within the half-light radius, the sample of local galaxies have $600 \lesssim \mathrm{S/N} \lesssim 3000$. The intermediate redshift galaxies in Paper II have S/N in the range 40 to 90, with a mean of ~ 55. This is sufficiently high that we focus our attention here on the effects of spatial sampling and resolution.

Even in the absence of significant image aberrations, an additional limiting factor is the number of resolution elements sampling the inner radius. This is likely to become a limiting factor when the half-light radii is only sampled by a few pixels. To understand this potential systematic, we have calculated six concentration indices $C = 5\log(r_o/r_i)$ for several different choices of inner and outer radii. We use r_i enclosing 20% and 30% of the light and r_o enclosing 50%, 70%, and 80% of the light. The radii were measured for nearby galaxies that were block-averaged by factors 2, 4, and 6 to simulate coarser spatial sampling, as shown in Figure 8. The six different concentration indices are plotted as a function of sampling in Figure 9. These simulations span sufficient dynamic range in size to cover most galaxies observed, for example, in the Hubble Deep Field. With factors of 4 and 6, we measure radii with pixel sampling similar to that observed in the *HST* WFPC2 images of the intermediate-redshift objects of Paper II. Typically, these galaxies have half-light radii of 0″.3–0″.7. For the Planetary Camera, the scale is 0″.046 pixel^{-1} and for the Wide Field,

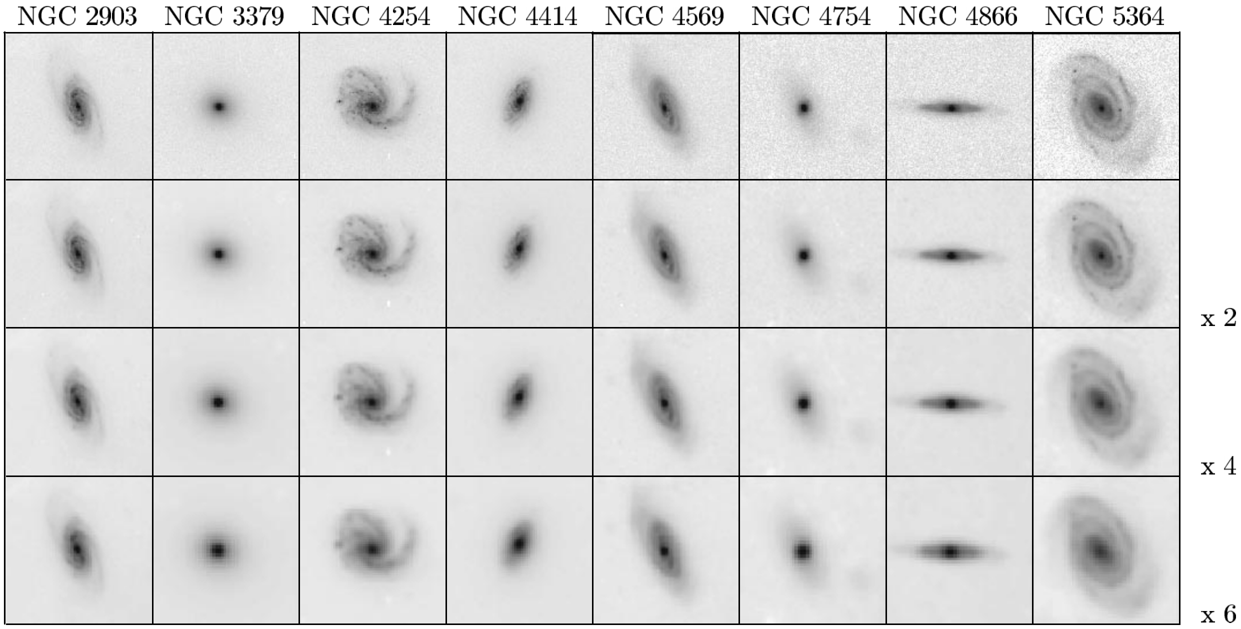

FIG. 8.—Representative subset of galaxy images from the Frei et al. catalog, block-averaged by factors 1, 2, 4, and 6 (*top to bottom*). While the apparent change in qualitative (visually assessed) morphology is small, the effects on the quantitative parameters C and A can be substantial. Half-light radius and surface brightness are only weakly affected.

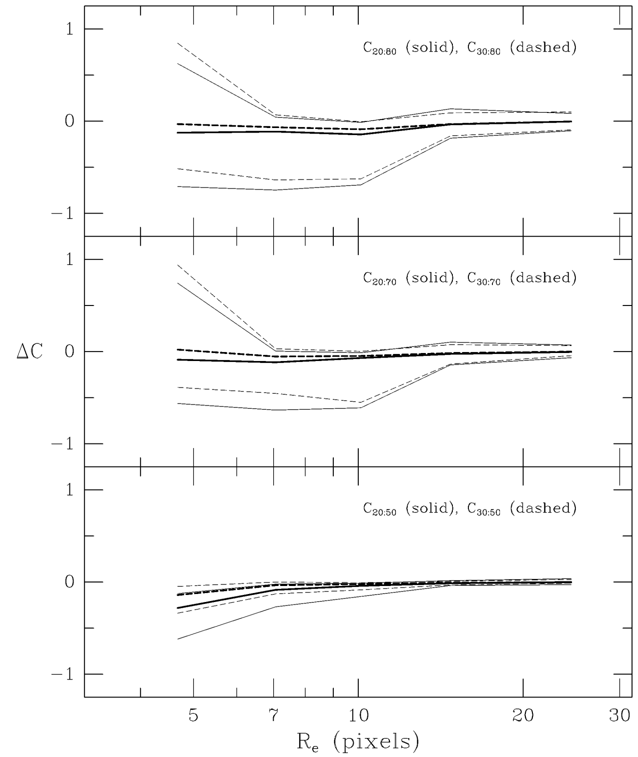

FIG. 9.—Resolution dependence of image concentration, C, for the galaxies in the Frei et al. catalog: ΔC vs. the half-light radius R_e (in pixel units of the block-averaged images). ΔC is the difference between the concentration index for a given simulated value of R_e relative to the original concentration value (i.e., that value measured on the observed image). Measurements for six definitions of the concentration index are plotted (two types per panel, labeled by line type). The central line (*heavy*) is the median value of this difference, and the bounding lines are the 25% and 75% values, i.e., 50% of the simulations are contained between the top and bottom lines for each index.

0″.10 pixel^{-1}; hence, the half-light radii are of order 3 to 15 pixels.

The half-light radius $r(50\%)$ is remarkably stable, even with poor sampling. Unfortunately, the dynamic range given by concentration indices with $r_o = r(50\%)$ is too small to be useful. As expected, the 30% radius was more stable than the 20% radius to decreased spatial resolution. However, the concentration indices using $r(30\%)$ were less sensitive to the differences between galaxy types and gave a smaller dynamic range than indices using $r(20\%)$. The inner radius dominated the effect on the amplitude of the systematics; changing the outer radius from 70% to 80% decreased the scatter only marginally. With a block-averaging factor of 6, where the half-light radii are typically only ∼5 pixels, the scatter becomes large for all choices of concentration indices.

Based on these simulations, we decided to use the radii enclosing 80% and 20% of the total light (as did Kent 1985), even though $r_o = r(70\%)$ gives concentration indices with slightly smaller scatter at poor resolution. For objects with half-light radii of only 7 pixels, the mean differences in concentration (relative to the original image) are $\Delta C_{80:20} = -0.10^{+0.20}_{-0.60}$ and $\Delta C_{70:20} = -0.10^{+0.15}_{-0.50}$. Even at a resolution of only 5 pixels per half-light radius, the concentration index only deviates by 0.2 relative to the original image; this is ∼8% of the dynamic range in $C_{80:20}$. Thus we consider this parameter to be robust enough to useful in the comparison of local and intermediate-redshift samples.

A2. SYSTEMATICS WITH WAVELENGTH

Observations at different wavelengths sample preferentially different stellar populations in a galaxy. Since these populations are not always spatially homogeneous, the image-structural characteristics (concentration, asymmetry, and half-light radius) will have some wavelength dependence (e.g., see de Jong's 1995 study of disk scale lengths). Hence, when comparing one of these parameters for different galaxies, the parameter ideally should be measured at the same rest-frame wavelength for all objects. This is not possible in general for studies over a wide range in redshifts employing a finite number of observed bands. To determine the amplitude of the wavelength-dependence for the measured structural parameters, we therefore compare the B_J and R structural parameters for 72 of the Frei et al. galaxies. The differences between the red and blue structural parameters versus the rest-frame color $B-V$ are shown in Figure 10. For comparison, all intermediate-redshift objects in Paper II, except two, fall in the bluest bin ($B-V < 0.62$).

The plot of $\Delta C = C_B - C_R$ shows that in most cases, the values are slightly negative, i.e., the majority of objects are more highly concentrated in the red band than in the blue, as expected because of the redness of the central bulge. Only the bluest galaxies have comparable image concentration in both bands. There is a weak trend toward more negative values for the redder (early type) objects, which also show a larger scatter than the bluer objects.

In the plot of $\Delta A = A_B - A_R$ it is clear that most galaxies have positive values, i.e., their image structure is more asymmetric in the blue band than in the red, as shown by

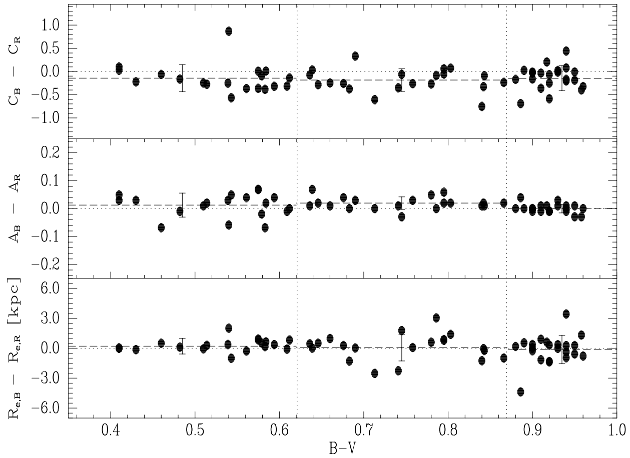

FIG. 10.—Wavelength dependence of structural parameters for galaxies in the Frei et al. sample, plotted vs. galaxy rest-frame color. Dashed lines show the mean differences between blue and red bands and the error bars show the 1 σ dispersions for three bins in color: $B-V < 0.62$ (late type), $0.62 < B-V < 0.87$ (intermediate type), and $B-V > 0.87$ (early type). *Top*: Image concentration $C_B - C_R$. Nearly all galaxies are more highly concentrated in the red band than in the blue and thus fall below the dotted line at $C_B - C_R = 0$. This difference is slightly larger for galaxies with intermediate-type morphology. *Middle*: Image asymmetry $A_B - A_R$. Late- and intermediate-type galaxies are more asymmetric in the blue band than in the red band. Red objects are generally very symmetric in both bands and have $A_B - A_R \sim 0$. This panel can be compared with Fig. 2 in Conselice et al. (2000), where $A_B - A_R$ is plotted vs. A_R. Since asymmetry and color are strongly correlated for the Frei et al. sample (as seen in Fig. 3), the trend in Conselice's plot is similar to what is shown here. *Bottom*: Half-light radius $R_{e,B} - R_{e,R}$. Although the scatter in this diagram is relatively large, it is clear that the half-light radius shows little wavelength dependence over this wavelength range (see de Jong 1995). Objects with blue $B-V$ color tend to be slightly larger in the blue band than in the red.

Conselice (1997). The difference in asymmetry is only seen for late- and intermediate-type objects; red objects are generally very symmetric in both bands and have $A_B - A_R \sim 0$. This trend was also noted by Brinchmann et al. (1998).

The plot of half-light radii ($\Delta R_e = R_{e,B} - R_{e,R}$) shows that most values are slightly positive, with a larger scatter for redder objects. Little trend with color is seen. The fact that the galaxies have slightly larger half-light radii in the blue band is consistent with their image concentration being higher in the red band, as a bulge profile generally has a much smaller scale length than an exponential profile.

In summary, the average differences ($\pm 1\ \sigma$) between parameters for galaxies with $B - V < 0.62$, determined from the B_J and R bands, are: $\Delta C = -0.15 \pm 0.30$, $\Delta A = 0.013 \pm 0.044$, and $\Delta R_e = 0.21 \pm 0.80$ kpc.

A2.1. *Corrections for Wavelength Systematics*

Based on the mean values above, we correct the measured structural parameters for galaxies at nonzero redshift to the rest-frame B-band values as follows, where for clarity we use the intermediate redshift galaxies in Paper II as an example. The structural parameters of these intermediate-redshift objects generally were measured at rest-frame wavelengths between B_J and R, i.e., in the observed WFPC2 I_{814} band for $z \sim 0.6$. For "normal" galaxies, this would cause us to overestimate C, and underestimate A and R_e. Hence we use the differences listed above and the redshift of the objects to linearly interpolate the correction to the measured values. Specifically, for a given parameter and color bin, we use the mean difference between values measured in the B_J and R bands and the position of the rest-frame wavelength relative to the B_J band to make corrections to the measured parameters. (Note that the correction made to R_e also affects the value of SB_e in general.) For some objects, the combination of observed bandpass and redshift corresponds to rest-frame wavelengths slightly blueward of B_J. When computing the corrections for these objects, we assumed that the wavelength trends continue outside the B_J–R wavelength range. Overall, these corrections are small for objects in Paper II, while for higher redshift objects we expect band-shifting effects to become increasingly important.

We add a final, cautionary note that it is not certain the corrections for intermediate-redshift objects should be made based on the correlations we see for the nearby sample. When comparing the observations in the bluer bands (B_{450} or V_{606}) to those in, e.g., the I_{814} used in Paper II, we find that most objects are more concentrated in the blue band and slightly larger in the red band—this is the opposite of what we see for the Frei et al. sample.[7] For asymmetry, the trend is the same for both samples (higher A in bluer bands). The trends are not directly comparable, however, to what we see in the local sample, as the observations in the bluer bands correspond to rest-frame wavelengths in the UV region for most intermediate-redshift galaxies. For this reason, and since the small sample of intermediate-z objects poorly defines the variation in image structure with wavelength, we adopt the more well-determined trends seen for the Frei et al. sample to calculate the band-shifting corrections. These corrections based on local galaxy trends tend to make the intermediate-redshift objects somewhat less "extreme"; their half-light radii become larger, their surface brightnesses fainter, and their image concentrations lower. If instead we had based our corrections on the trends seen within the intermediate-z sample of Paper II, then this sample would be even more extreme relative to the local galaxy sample. The corrections would then tend to shift the positions of the intermediate-z objects even farther from the nearby galaxies in diagrams that include any of the parameters R_e, SB_e, and C.

A3. SYSTEMATICS WITH APERTURE SHAPE

A3.1. *Comparison with Elliptical Aperture Photometry*

Circular-aperture surface photometry will yield systematic differences in the measured structural parameters when compared to those derived from elliptical-aperture surface photometry. To assess this, we compared our results for the Frei et al. catalog in R and r bands to the results of Kent (1985) for a sample of local Hubble-type galaxies (Fig. 6). Kent used elliptical apertures tailored to fit the axis ratio and position angle of each isophote in galaxy images to determine r band image concentration and average surface brightness within the half-light radius.

As we detail in the figure caption, we have attempted to transform all of the surface brightness values to the Cousins R band (R_c). For each of the relations in Figure 6 we have characterized the slopes and scatter about a mean regression using a simple linear, least-squares algorithm with an iterative, sigma-clipping routine to remove outlying points. Given the nature of the data, such an algorithm is not statistically correct (see, e.g., Akritas & Bershady 1996). However, given the potential photometric uncertainties (discussed below) and the need for robust estimation, it is not possible to formally implement more appropriate algorithms at this time. Nonetheless, the relative characterization of the slopes and scatter between Frei et al. and Kent samples is useful.

As discussed in § 4.1.3, the slope of the correlation between average surface-brightness and image concentration is steeper for our study than for Kent's because of a decreased range in image concentration in our study. The effect (*bottom panel*, Fig. 6) is such that the bluest galaxies have comparable image concentration values in both studies while the image concentration of the reddest galaxies differ by as much as 1 unit in the mean (Kent's values are larger). We interpret this as likely to be the effect of different aperture shapes. The results of our study of systematics with axis ratio (below) support this conclusion. Surprisingly, there is no indication that elliptical apertures give significantly different results than circular apertures for intermediate- and late-type (disk-dominated) galaxies.

The larger scatter in the Frei et al. (1996) sample in the top two panels of Figure 6 might lead one to conclude that the elliptical apertures provide a superior measurement of effective surface brightness. However, much of the scatter is due to the subset of the Frei et al. sample observed at Palomar Observatory. We believe that zero-point problems are the cause of much of this scatter, consistent with discussion in Frei et al. concerning the difficulty of photometric calibration. The bulk of the objects observed at

---

[7] Indeed, Huchra noted that the Markarian galaxies get bluer toward their centers, reminiscent of the blue "bulges" seen in the blue nucleated galaxies of Paper II, yet in contrast to the color gradients found for "normal" galaxies. This type of color-aperture relation was also noted by de Vaucouleurs (1960, 1961) for the latest Hubble-type galaxies (Sm, Im).

Lowell Observatory are consistent with independent R_c-band photometry from Buta & Williams (1996), although there are some points that are very discrepant. In general, the overlap is excellent in SB_e and $B-V$ between the Kent sample, the Lowell subset of the Frei et al. sample, and the subset of the Frei et al. sample with Buta & Williams's photometry.

A3.2. *Systematics with Axis Ratio*

A second approach to determine the systematic effects of aperture shape on measured structural parameters was also used: we quantify the degree to which "normal" galaxies with the same intrinsic morphology but with different axial ratios a/b will have different C when measured with circular apertures. The galaxies in the Frei et al. catalog were divided into early-, intermediate- and late-type objects (using the same bins as elsewhere in the paper), and we plot concentration and half-light radius versus the logarithm of the axis ratio (taken from the RC3 catalog).

In the image concentration plots (Fig. 11), a weak trend can be seen for the late-type galaxies (*top panel*), with slightly higher values of C for the more inclined objects. This effect, if caused by the shape of the apertures, will lead us to overestimate the image concentration by at most ~ 0.1 (3%) for the nearly edge-on galaxies. We do not expect this to be a problem for our analysis. The two labeled objects have unusually high values of C for their morphological type. One of them, NGC 5033, is known to be a Seyfert 1 galaxy; the other, NGC 4651, is a suspected "dwarf Seyfert" galaxy (Ho et al. 1997). For intermediate-type objects (*middle panel*) no trend is observed. The lowest C-value, which belongs to NGC 4013, could be caused by the prominent dust lane in this object: the central light distribution is divided into two parts, making it difficult to determine the position of the center. Effects like these will likely be more problematic for objects with high values of a/b. The highest C-value in this plot is that of NGC 4216, which also is highly inclined and has spiral arm dust lanes superposed on the bulge. In the bottom panel, a trend is observed for the early-type galaxies: the concentration is lower for objects with higher a/b ratio. This effect will cause us to underestimate the image concentration of these objects by ~ 0.5, or 10%–15%. This result agrees well with what was seen in the comparison of the Frei et al. sample to Kent's image concentration measurements, as described above. This leads us to conclude that our circular aperture photometry will underestimate the image concentration somewhat for elliptical/S0 galaxies. Again, there is no indication that the aperture shapes lead to different results for intermediate- and late-type galaxies.

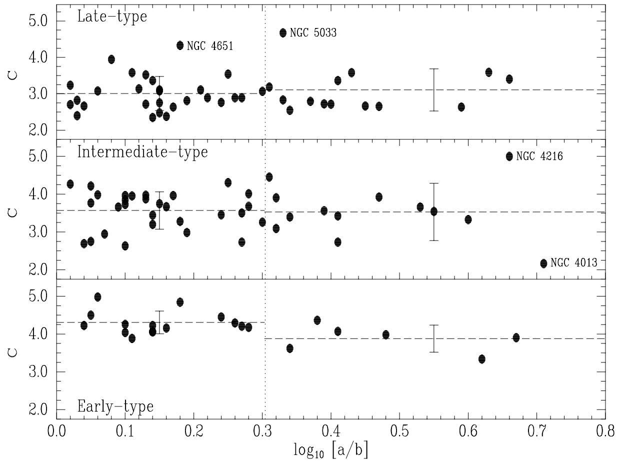

FIG. 11.—Axis ratio dependence of image concentration C for galaxies of different morphological types in the Frei et al. sample. The dotted line separates the sample into two bins at $\log_{10}(a/b) = 0.3$, corresponding to an inclination of 60°. The dashed lines and error bars show the mean and 1σ dispersion for each morphological type and bin. Labeled objects are discussed in the text. *Top*: Late-type objects with high inclination have slightly higher measured C than more face-on objects. *Middle*: For intermediate-type galaxies the measured concentration indices show no correlation with the axial ratio (a/b). *Bottom*: For early-type galaxies, a tendency can be seen where objects with larger axial ratio (a/b) are measured to have lower image concentration.

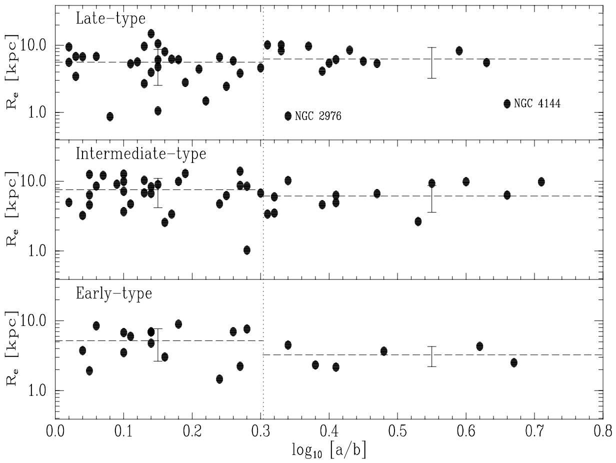

FIG. 12.—Axis ratio dependence of half-light radius R_e for galaxies of different morphological types in the Frei et al. sample. The dotted line separates the sample into two bins at $\log_{10}(a/b) = 0.3$, corresponding to an inclination of 60°. The dashed lines and error bars show the mean and 1 σ dispersion for each morphological type and bin. *Top*: Measured R_e are slightly larger for late-type objects with high axial ratios. *Middle*: Intermediate-type objects have somewhat smaller R_e for high values of (a/b). In both of these panels the scatter is large and the differences between the bins are small. *Bottom*: Early-type galaxies with larger axial ratio (a/b) are measured to have $\lesssim 30\%$ smaller half-light radii.

In the plots of half-light radius R_e versus a/b (Fig. 12), no trends are seen for the intermediate- and late-type objects. For the early-type objects, however, the measured half-light radii become progressively smaller for increasing values of a/b. The trend is weak; it will cause us to underestimate the half-light radii by at most 30% for objects with $a/b \sim 4$. If this effect is real, the derived surface brightness will be too bright by $\lesssim 0.7$ mag for the most highly elliptical early-type galaxies.

REFERENCES

Aaronson, M. 1978, ApJ, 221, L103

Abraham, R. G., Tanvir, N. R., Santiago, B. X., Ellis, R. S., Glazebrook, K., & van den Bergh, S. 1996a, MNRAS, 279, L47

Abraham, R. G., Valdes, F., Yee, H. K. C., & van den Bergh, S. 1994, ApJ, 432, 75

Abraham, R. G., van den Bergh, S., Glazebrook, K., Ellis, R. S., Santiago, B. X., Surma, P., & Griffiths, R. E. 1996b, ApJS, 107, 1

Akritas, M. G., & Bershady, M. A. 1996, ApJ, 470, 706

Bershady, M. A. 1995, AJ, 109, 87

———. 1999, Toward a New Millennium in Galaxy Morphology, ed. D. L. Block, I. Puerari, A. Stockton, & D. Ferreira (Dordrecht: Kluwer), in press

Bingelli, B., & Cameron, L. M. 1991, A&A, 252, 27

Bingelli, B., & Jerjen, H. 1998, A&A, 333, 17

Brinchmann, J., et al. 1998, ApJ, 499, 112
Bromley, B. C., Press, W. H., Huan, L., & Krishner, R. P. 1998, ApJ, 505, 25
Burda, P., & Feitzinger, J. V. 1992, A&A, 261, 697
Buta, R., & Williams, K. L. 1996, AJ, 109, 543
Caldwell, N. 1983, AJ, 88, 804
Connolly, A. J., Szalay, A. S., Bershady, M. A., Kinney, A. L., & Calzetti, D. 1995, AJ, 110, 1071
Conselice, C. 1997, PASP, 109, 1251
Conselice, C., Bershady, M. A., & Jangren, A. 2000, ApJ, 529, 886
Couch, W. J., Ellis, R. S., Sharples, R. M., & Smail, I. 1994, ApJ, 430, 121
de Jong, R. S. 1995, Ph.D. thesis, Univ. Groningen
———. 1996a, A&A, 313, 45
———. 1996b, A&AS, 118, 557
de Vaucouleurs, G. 1960, ApJ, 131, 574
———. 1961, ApJS, 5, 233
de Vaucouleurs, G., de Vaucouleurs, A., & Corwin, H. G. 1976, Second Reference Catalogue of Bright Galaxies (Austin: Univ. Texas Press)
de Vaucouleurs, G., de Vaucouleurs, A., Corwin, H. G., Buta, R. J., Paturel, G., & Fouqué, P. 1991, Third Reference Catalog of Bright Galaxies (New York: Springer) (RC3)
Djorgovski, S., & Spinrad, H. 1981, ApJ, 251, 417
Doi, M., Fukugita, M., & Okamura, S. 1993, MNRAS, 264, 832
———. 1983, ApJ, 270, 7
Dressler, A., & Gunn, J. E. 1992, ApJS, 78, 1
Driver, S., Fernandez-Soto, A., Couch, W. J., Odewahn, S. C., Windhorst, R. A., Phillips, S., Lanzetta, K., & Yahil, A. 1998, ApJ, 496, L93
Driver, S., Windhorst, R. A., & Griffiths, R. E. 1995, ApJ, 453, 48
Elmegreen, D. M., & Elmegreen, B. G. 1982, MNRAS, 201, 1021
Folkes, S. R., Lahav, O., & Maddox, S. J. 1996, MNRAS, 283, 651
Freeman, K. C. 1970, ApJ, 160, 811
Frei, Z., & Gunn, J. E. 1994, AJ, 108, 1476
Frei, Z., Guhathakurta, P., Gunn, J. E., & Tyson, J. A. 1996, AJ, 111, 174
Gallagher, J., & Hunter, D. 1987, AJ, 94, 43
Han, M. 1995, ApJ, 442, 504
Ho, L. C., Filippenko, A. V., Sargent, W. L. W., & Peng, C. Y. 1997, ApJS, 112, 391
Hubble, E. 1936, The Realm of the Nebulae (New Haven: Yale Univ. Press)
Huchra, J. P. 1977a, ApJS, 35, 171
———. 1977b, ApJ, 217, 928
Humason, M. L., Mayall, N. U., & Sandage, A. R. 1956, AJ, 61, 97
Jangren, A., Bershady, M. A., Conselice, C., Koo, D. C., & Guzmán, R. 2000, AJ, submitted (Paper II)
Kent, S. M. 1984, ApJS, 56, 105
Kent, S. M. 1985, ApJS, 59, 115
Kron, R. G. 1995, in The Deep Universe, ed. B. Bingeli & R. Buser (New York: Springer), 233
Marleau, F. R., & Simard, L. 1998, ApJ, 507, 585
Marlowe, A. T., Meurer, G. R., Heckman, T. M., & Schommer, R. 1997, ApJS, 112, 285
Mobasher, B., Ellis, R. S., & Sharples, R. M. 1986, MNRAS, 223, 11
Morgan, W. W. 1958, PASP, 70, 364
———. 1959, PASP, 71, 394
Naim, A., Lahav, O., Sodre, L., Jr., & Storrie-Lombardi, M. C. 1995, MNRAS, 275, 567
Odewahn, S. C. 1995, PASP, 107, 770
Odewahn, S. C., Windhorst, R. A., Driver, S. P., & Keel, W. C. 1996, ApJ, 472, L13
Okamura, S., Kodaira, K., & Watanabe, M. 1984, ApJ, 280, 7
Petrosian, V. 1976, ApJ, 209, L1
Ronen, S., Aragón-Salamanca, A., & Lahav, O. 1999, MNRAS, 303, 284
Salzer, J. J., Macalpine, G. M., & Boroson, T. A. 1989, ApJS, 70, 479
Sandage, A. R. 1961, The Hubble Atlas of Galaxies (Washington: Carnegie Inst. Washington)
Sandage, A. R., & Bedke, J. 1993, Carnegie Atlas of Galaxies (Washington: Carnegie Inst. Washington)
Sandage, A. R., & Perelmuter, J.-M. 1990, ApJ, 350, 481
Sandage, A. R. & Tamman, G. A. 1987, A Revised Shapely-Ames Catalog of Bright Galaxies (Washington: Carnegie Inst. Washington)
Schade, D., Lilly, S. J., Crampton, D., Hammer, F., Le Fèvre, O., & Tresse, L. 1995, ApJ, 451, L1
Schade, D., Lilly, S. J., Le Fèvre, O., Hammer, F., & Crampton, D. 1996, ApJ, 464, 79
Serra-Ricart, M., Calbet, X., Garrido, L., & Gaitan, V. 1993, AJ, 106, 1685
Simard, L. 1998, in ASP Conf. Ser. 145, Astronomical Data Analysis Software Systems VII, ed. R. Albrecht, R. N. Hook, & H. A. Bushouse (San Francisco: ASP), 108
Simard, L., et al. 1999, ApJ, 519, 563
Spiekermann, G. 1992, AJ, 103, 2102
Storrie-Lombardi, M. C., Lahav, O., Sodre, L., Jr., & Storrie-Lombardi, L. J. 1992, MNRAS, 259, P8
Tully, R. B. 1988, Nearby Galaxies Catalogue (Cambridge: Cambridge Univ. Press)
Watanabe, M., Kodaira, K., & Okamura, S. 1985, ApJ, 292, 72
Whitmore, B. C. 1984, ApJ, 278, 61
Wirth, G. D., Koo, D. C., & Kron, R. G. 1994, ApJ, 435, L105
Wyse, R. F. G., Gilmore, G., & Franx, M. 1997, ARA&A, 35, 637
Zaritsky, D., Zabludoff, A. I., & Willick, J. A. 1995, AJ, 110, 1602